Heliyon 9 (2023) e21862

Contents lists available at ScienceDirect

Heliyon

journal homepage: www.cell.com/heliyon

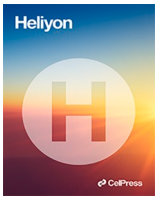

Preparation of chemically and thermally modified water caltrop epicarp (*Trapa natans* L.) adsorbent for enhanced adsorption of Ni (II) from aqueous solution

Muhammad Zobayer Bin Mukhlish *, Shekh Nazibunnesa, Shariful Islam, Abu Saleh Al Mahmood, Md Tamez Uddin

Department of Chemical Engineering and Polymer Science, Shahjalal University of Science and Technology, Sylhet, 3114, Bangladesh

ARTICLE INFO

Keywords:
Trapa natans L.
Ni(II) ion
Adsorption
Isotherm
Kinetics
Modified adsorbent

ABSTRACT

The present study aims to prepare waste water caltrop (Trapanatans L.) epicarp (WCS)-based adsorbents such as raw WCS (WCS-Raw), citric acid-grafted WCS (WCS-CA), acrylamide-grafted WCS (WCS-AM), and calcined WCS (WCS–Si) for Ni(II) removal from aqueous solution in batch adsorption process. The physical and chemical properties of the prepared adsorbents were investigated by different characterization techniques such as scanning electron microscopy (SEM), Fourier-transform infrared (FTIR) spectroscopy, nitrogen adsorption-desorption analyses, and pH at the Point of Zero Charge (pHpzc) in order to assess the suitability and effectiveness of the adsorbents for the removal of Ni(II) by understanding their surface morphology, chemical composition, porosity, and surface charge properties. The experimental Ni(II) adsorption data followed both the Langmuir isotherm and the pseudo-second-order kinetic model suggesting the adsorption process on the prepared adsorbents is well-described by these models. The modified adsorbents WCS-CA, WCS-AM, and WCS-Si exhibited a maximum adsorption capacity of 52.08, 40.32, and 158.73 mg/g, respectively, while WCS-Raw had a capacity of 29.06 mg/g. The thermodynamic study revealed that the adsorption process was feasible, spontaneous, and endothermic. The desorption study demonstrated that the adsorbents could be reused for multiple cycles with minimal loss of activity. The present work evidenced the potential practical applicability and sustainability of the WCS-based adsorbents as promising adsorbents in treating and removing Ni(II) from wastewater.

1. Introduction

Rising industrialization is causing significant stress on our water environment, reducing the availability of clean water, which is crucial for aquatic life, ecology, human health, and a thriving economy [1]. Both humans and other living things are seriously at risk from water contamination caused by numerous toxins, such as heavy metal ions, dyes, pesticides, chemical compounds, bacteria, and viruses. Several processes, including mining, soil erosion, weathering of rocks and minerals, electroplating, nuclear power plant operations, and the manufacturing of semiconductors, paper, ceramics, textiles, leather, and batteries, can release heavy metal ions, such as Ni^{2+}, Cr^{6+}, Pb^{2+}, Cd^{2+}, Zn^{2+}, As^{3+}, and Hg^{2+}, into the environment and end up in water bodies [2–5]. Aquatic species, fish, and

* Corresponding author.
E-mail address: zobayer-cep@sust.edu (M.Z.B. Mukhlish).

https://doi.org/10.1016/j.heliyon.2023.e21862
Received 5 June 2023; Received in revised form 27 October 2023; Accepted 30 October 2023
Available online 2 November 2023

humans at the top of the food chain can all accumulate these toxic metal ions that are present in wastewater. Bioaccumulation of these ions in the human body can also occur through drinking water.

Nickel, a transition element widely present in the environment, has been taken into account in the present work. The US EPA has set specific nickel limits for wastewater effluent reuse, ranging from 0.2 mg/L for long-term reuse to 2 mg/L for short-term reuse [3,6,7]. Nickel may be advantageous as an activator of some enzyme systems in trace amounts and is known to participate in biological activities such as respiration, metabolism, and biosynthesis; its intake in higher concentrations creates adverse health effects and causes different types of diseases, including gastrointestinal manifestations, pulmonary fibrosis, lung and bone cancer, renal edema, chronic asthma, skin dermatitis, and central nervous system dysfunction [3,8,9]. Furthermore, it is a teratogen and may cause malformations in embryos [10]. Hence, the removal of Ni(II) from wastewater is a major issue.

Different techniques such as solvent extraction, ion exchange, electrochemical treatment, chemical precipitation, filtration, oxidation/reduction, membrane technologies, and evaporation recovery have been used to remove Ni(II) ions from aqueous solutions; however, most of these techniques are costly or produce toxic waste products [5,8,11–16]. Adsorption is one of the most effective techniques, offering several advantages, such as very effective metal extraction from diluted solutions, a reduction in secondary waste, ease of operation, and the ability to recover adsorbed metals for recycling or reuse [17,18]. Adsorbents like activated carbon, metal nanoparticles, and graphene are commonly used but are expensive and have poor recycling potential [19]. It is necessary to investigate a cheap, conveniently accessible, high-adsorption capacity adsorbent for heavy metal removal [20,21]. In this context, agricultural wastes and some other living or nonliving biomasses present a viable alternative as inexpensive adsorbents for the treatment of heavy metal-containing wastewater [16,20,22]. However, the use of these materials is limited due to issues such as poor metal removal efficiency and low biosorption dynamic sites [23].

Nowadays, the emphasis lies on chemically or thermally modified agricultural waste for enhancing metal ion removal from aqueous medium. Lignocellulosic agricultural wastes contain reactive functional groups like phenolic, carbonyl, hydroxyl, amino, acetamido, and sulfhydryl groups [2,24–26]. Chemical and thermal modification of waste biomass can enhance their functional group potential, thereby increasing the metal binding capacity of these biosorbents [2,27–30]. For example, the adsorption capacity of Trapanatan Biopolymer for Co(II) was improved by $KMnO_4$ treatment [30]. Chemical treatment using HNO_3, $HClO_4$, and H_2O_2 considerably enhanced the adsorption capacity of Trapabispinosa'speel for Pb(II) [31]. Thermal treatment of rice husk improved its sorption capacity for Pb(II) [32]. Various waste biomaterials, including citric acid-functionalized aloe vera leaf powder [19], Na_2CO_3-modified steam-heated aloe vera leaf [33], aloe vera waste leaves [34], lemon peel, cassava peel [35], sawdust [22], algae [20], tea waste [36], rice straw [37], tamarind bark [38], oil cake [39], litchi chinensis seeds, and caesalpiniabonducella seed [40], have been studied as adsorbents to remove nickel from wastewater.

Agricultural waste, such as Trapa natans L. fruit epicarp-based adsorbents can be a great choice for removing nickel ions from wastewater. Native to Europe, Asia, and Africa, *Trapa natans* L. is a little free-floating plant growing primarily in shallow water or swampy regions and is also known as the water chestnut, water caltrop, or singhara in India and Bangladesh. It is extensively cultivated for edible seeds in many countries, including China, Taiwan, India, and Bangladesh [41–43]. The *Trapa natans* L fruit contains an inner edible kernel covered with a thick outer epicarp. The average weight of the fruit is about 10.28 g, and the epicarp contains about 50 wt % of the whole fruit [44]. Tens of thousands of metric tons of water caltrop epicarp or shell (WCS) are generated during the postharvest period and often dumped in farmlands or occasionally used as organic fertilizer in Asian countries [45]. It is important to study the conversion of such waste biomass into value-added products, such as adsorbents for the remediation of heavy metal contamination in wastewater. Reports on the reuse of Trapanatans L.'s epicarp as a valuable material are very few in the literature [45]. The WCS was used as an adsorbent for the removal of dyes [46,46,47], and a few heavy metals, e.g. Cu (II) [48], Cr(VI) [49], and Co(II) [30].

Although there are several studies in the literature on producing raw and modified adsorbents from agricultural waste, there is no published report on producing water caltrop epicarp (WCS)-based adsorbents through calcination or treatment with citric acid and acrylamide for heavy metal removal. The present work aimed to prepare biosorbents using water caltrop epicarp through chemical treatment with citric acid and acrylamide, as well as thermal treatment, to adsorb Ni(II) from aqueous solutions. The morphological and textural characteristics of the materials were studied using a variety of characterization techniques, including field emission scanning electron microscopy, Fourier transform infrared spectroscopy, and N_2 adsorption-desorption isotherm. Key parameters affecting the adsorption process, such as adsorbent dosage, pH, metal ion concentration, and contact time, were examined. This study also explored adsorption isotherm and kinetic models, investigated reusability characteristics of adsorbents, and compared the adsorption performances of raw and modified adsorbents.

2. Materials and methods

2.1. Reagents and stock solution

All of the compounds employed in this study were of analytical grade and were not further purified before usage. Citric acid and acrylamide were purchased from Techno pharm chem India. Hydrochloric acid, sodium hydroxide, and $NiCl_2.6H_2O$ were obtained from MERCK, Germany. Working solutions were produced by appropriately diluting the prepared stock solution of Ni(II) (1 g/L), which was made by dissolving a weighed quantity of $NiCl_2.6H_2O$ in deionized water.

2.2. Preparation of adsorbents

2.2.1. Preparation of raw WCS adsorbent (WCS-Raw)

Water caltrop (epicarp) shells (WCS), collected from a local fruit processing industry (in Sylhet district, Bangladesh), were thoroughly washed with distilled water several times to remove dirt and earthy materials and then boiled for 30 min, followed by washing again with distilled water until the water was colorless. The as-obtained WCS pieces were dried in an oven at 105 °C for 24 h and crushed into powder, followed by sieving in a sieve shaker. The particles in the range of 250–500 μm were used as raw adsorbent (WCS-Raw).

2.2.2. Pretreatment of WCS-Raw with alkali (WCS–NaOH)

The pretreatment of WCS-Raw with alkali involved immersing a 15-g WCS-Raw sample in an aqueous NaOH solution (0.5 mol/L) at 70 °C, stirring magnetically for 30 min, and then separating, washing, and drying at 50 °C for 12 h. The alkali-treated sample was labeled as WCS-NaOH, a precursor for CA- and AM-modified WCS adsorbents.

2.2.3. Preparation of citric acid-modified WCS adsorbent (WCS-CA)

Four hundred milligrams of potassium dihydrogen phosphate and 600 mg of citric acid (CA) were added into a suspension of 4 g of WCS-NaOH in 120 mL of distilled water and stirred for 1 h, which was then transferred to a closed container and heated at 150 °C for 3 h. Subsequently, the CA-treated WCS-NaOH was separated by centrifugation, rinsed with deionized water, and dried overnight at 90 °C in an oven. The dried sample as obtained was tagged as WCS-CA and kept in an airtight bottle for further use.

2.2.4. Preparation of acrylamide-modified WCS adsorbent (WCS-AM)

In a beaker, 2 g of WCS-NaOH and 0.55 g of potassium persulfate were mixed with 120 mL of deionized water, followed by heating at 80 °C under magnetic stirring for an hour (Suspension-1). Meanwhile, an acrylamide (AM) solution was prepared using 14 g of AM and 50 mL of deionized water and was added dropwise into Suspension-1, followed by heating at 80 °C for 4 h under magnetic stirring. After that, the AM-modified WCS was rinsed with deionized water for 15 min and dried in an oven at 90 °C for 12 h. The dried material was labeled as WCS-AM and stored for further use.

2.2.5. Preparation of calcined WCS adsorbent (WCS–Si)

A 10 % (w/v) hydrogen chloride solution was added to 60 g of WCS-Raw sample, which was then incubated at 90 °C for 1 h. After incubation, the solid residue was rinsed with deionized water, dried at 60 °C for 24 h, and then calcined in a muffle furnace at 800 °C for 48 h. The obtained ash was marked as WCS-Si.

2.3. Characterization of the adsorbent

Physicochemical properties such as bulk density, moisture content, volatile matter, ash, and fixed carbon of the WCS-Raw adsorbent were determined using the methods described elsewhere [1,50]. The acid value of WCS-Raw adsorbent was determined using the titration methods described in the literature [51]. One hundred milligrams of adsorbent were mixed with 5 mL of 0.1 N H_2SO_4 in 50 mL of distilled water and titrated using 0.1 N NaOH with phenolphthalein as an indicator.

The acid value (A_T) was calculated using Eq. (1):

$$A_T(mEqH^+/g) = \frac{(v_1 - v_0)\times 0.1}{m_0} \quad (1)$$

where v_1 is the volume (mL) of the 0.1 N NaOH titration solution used, v_0 is the volume (mL) of the 0.1 N NaOH solution used for neutralizing 5 mL of 0.1 N H_2SO_4 solution, and m_0 is the sample weight (g).

The surface morphology of the WCS samples was investigated using a scanning electron microscope (EVO 18, ZEISS, Germany). An ASAP 2020 Plus porosimetry analyzer (Micromeritics Instrument Corporation, USA) was used to record the nitrogen adsorption-desorption isotherms of the adsorbents at 77 K. The samples were degassed for 10 h at 120 °C under ultra-high vacuum before the measurement. The Brunauer-Emmett-Teller (BET) equation was used to calculate the specific surface areas (S_{BET}), and the Barrett-Joyner-Halenda (BJH) method was used to calculate the pore size distributions using adsorption branches of nitrogen adsorption-desorption isotherms. The Micromeritics software package was utilized for the calculation, employing the recurrent method and applying the Harkins and Jura equation for multilayer thickness. FTIR analysis was performed to identify the surface functional groups using an FTIR spectroscope (IRPrestige-21, Shimadzu, Kyoto, Japan). Samples were diluted with KBr and pressed into a disk shape for FTIR measurement. FTIR spectra were examined in the range of 400–4000 cm^{-1}.

The pH at the point of zero charge (pH_{pzc}) is an important property of a solid adsorbent in aqueous solutions because it gives an indication of the adsorption mechanism as well as the net surface charge on the adsorbent. The pHpzc of the adsorbent was determined by using the titration method described elsewhere [52,53]. In 100 mL of 0.1 M KNO_3 solution, 50 mg of adsorbent was added and stirred with a magnetic stirrer. After allowing the solution 10 min to reach equilibrium, the pH value was then determined by a pH meter (Model: HI2211, HANNA Instruments, Singapore). The titration was carried out with 0.1 M NaOH and 0.1 M HCl. The surface charge (Q) of adsorbent was calculated using Eq. (2) [52]:

$$Q = \frac{1}{w}(C_A - C_B - [H^+] - [OH^-]) \quad (2)$$

where w is the dry weight of adsorbent in aqueous system (g/L), C_A is the concentration of added acid in aqueous system (mole/L), C_B is the concentration of added base in aqueous system (mole/L), $[H^+]$ is the concentration of H^+ (mole/L), and $[OH^-]$ is the concentration of OH^- (mole/L). The pHpzc of the adsorbent was determined to be the pH corresponding to the Q value of zero.

2.4. Batch adsorption studies

Batch adsorption experiments were conducted to explore the impact of adsorbent dose, solution pH, metal ion concentration, and contact time on the removal of Ni (II) from aqueous solution. In the sorption experiment, a pre-weighed amount of adsorbent was mixed with 200 mL of Ni (II) solution in a 250 mL conical flask. Then the solid-solution mixture was agitated using a flash shaker at a constant oscillation of 500 rpm (Stuart Scientific Co. Ltd., Model SF1, U.K.). After adsorption, the adsorbent was removed from the solution, and the amount of Ni(II) in the supernatant liquid was estimated using an inductively coupled plasma-optical emission spectrometer (ICP-OES) (Model: AVIO-200). ICP-OES employs a high-temperature plasma to evaporate and excite the metal atoms in a liquid sample. The intensity of light emitted by the plasma at a specific wavelength for each element is measured and used to estimate the concentration of the concerned elements. The relationship between light intensity and element concentration in the sample is linear.

The effect of adsorbent dose was examined at an initial Ni(II) concentration of 10 mg/L, pH 7, varying the adsorbent dose between 0.25 and 2.5 g/L. The effect of initial solution pH on the sorption of Ni(II) was studied by varying the solution pH, e.g., pH 3, pH 5, pH 6, pH 6.5, pH 7, and pH 7.5, at a constant adsorbent dose of 0.25 g/L. During the pH study, the initial Ni(II) solution concentration was maintained at 57.89 mg/L, 56.17 mg/L, 56.17 mg/L, and 58.29 mg/L for WCS-Raw, WCS-CA, WCS-AM, and WCS-Si, respectively. The pH of the solution was maintained at the required value using either 0.1 M HCl or NaOH.

The adsorption equilibrium studies were carried out by adding 0.05 g of adsorbent into 200 mL Ni(II) solution with different initial concentrations of 10–130 mg/L at a pH of 7. Following 12 h of shaking at 25 °C, the Ni(II) concentrations in the sample were determined from the residual Ni(II) concentration in the supernatant liquid, as mentioned earlier. The procedures for kinetics studies were quite similar to the equilibrium tests. The kinetic experiments were carried out by adding 0.05 g of adsorbent in 200 mL of Ni(II) solution (pH 7) with initial concentrations of 50.94 mg/L for WCS-Raw and 54.78 mg/L for WCS-CA, WCS-AM, and WCS-Si. At specific intervals of time, the aqueous samples were withdrawn from the test solution for concentration measurements.

The adsorption density, defined as the amount of Ni(II) adsorbed per unit weight of adsorbent, was evaluated by using the following equations (Eq. (3) and Eq. (4)):

$$q_e = \frac{(C_0 - C_e)V}{W} \quad (3)$$

$$q_t = \frac{(C_0 - C_t)V}{W} \quad (4)$$

where q_e and q_t are the adsorption density (mg/g) at equilibrium and at time t, respectively. C_o, C_t, and C_e represent the liquid phase concentrations of Ni(II) (mg/L) at initial, at time t, and at equilibrium, respectively. V is the volume of solution (L), and W is the dry mass of adsorbent (g).

2.5. Adsorption isotherm studies

Adsorption isotherm studies are important for designing adsorbent-adsorbate systems and optimizing adsorbent use [54]. Langmuir [55], Freundlich [56], and Elovich [57] isotherm models were used to explain nickel ion adsorption onto WCS-based adsorbents. The Langmuir adsorption isotherm model is valid for the monolayer sorption of molecules onto the surface of the adsorbent with a finite number of identical sites without causing any steric hindrance or lateral interaction between the adsorbed molecules. The linear form of the Langmuir model is expressed as follows:

$$\frac{C_e}{q_e} = \frac{C_e}{q_m} + \frac{1}{q_m K_L} \quad (5)$$

where q_m denotes the maximum adsorption capacity (mg/g) and K_L indicates the adsorption equilibrium constant. The values of q_m and K_L can be computed from the slope and intercept of the linear plot of C_e/q_e versus C_e.

The Freundlich isotherm model signifies non-ideal adsorption and is not restricted to monolayer adsorption [58]. The linearized form of Freundlich isotherm can be presented by the following equation:

$$\ln q_e = \ln K_F + \frac{1}{n} \ln C_e \quad (6)$$

where K_F and n are the constants signifying the quantity of Ni(II) adsorbed on adsorbent for unit equilibrium concentration (i.e., $C_e = 1$) and the adsorption intensity, respectively. The value of 1/n is a measure of the adsorption intensity or surface heterogeneity. A value

of 1/n below one indicates a normal Langmuir isotherm, while 1/n above one is indicative of cooperative adsorption [59]. From the plot of $\ln q_e$ versus $\ln C_e$, K_F and $1/n$ values can be obtained.

The Elovich isotherm model [57] assumes that adsorption sites increase exponentially with loading, predicting multilayer adsorption. The Elovich isotherm equation is given as (Eq. (7)):

$$\ln\frac{q_e}{C_e} = \ln K_E q_{mE} - \frac{q_e}{q_{mE}} \tag{7}$$

where K_E is the Elovich equilibrium constant (L/mg) and q_{mE} is the Elovich maximum adsorption capacity (mg/g). The values of q_{mE} and K_E can be estimated from the slope and intercept of the linear plot of $\ln(q_e/C_e)$ versus q_e.

The Langmuir, Freundlich, and Elovich isotherm models do not provide information on the adsorption mechanism. The Dubinin-Radushkevich (D-R) model is used to reveal the adsorption mechanism by estimating the adsorption energy [34]. The linearized form of the Dubinin-Radushkevich isotherm equation is expressed as (Eq. (8)) [60,61]:

$$\ln q_e = -K_{DR}\varepsilon^2 + \ln q_m \tag{8}$$

where K_{DR} is the D-R isotherm constant related to the adsorption energy ($mol^2 \cdot kJ^{-2}$), q_m is the theoretical saturation capacity, and ε is the adsorption potential ($kJ \cdot mol^{-1}$) and can be expressed as (Eq. (9) and (10)):

$$\varepsilon = RT\ln\left(1+\frac{1}{C}\right) \tag{9}$$

$$C = C_e/C_s \tag{10}$$

where R is the gas constant (8.314 J K^{-1} mol^{-1}), T is the absolute temperature (298.15 K), and C_e and C_s are the equilibrium concentration and solubility of the adsorbate, respectively. In this work, C_s is 2540 g/L H_2O [62].

The mean free energy of adsorption (E), defined as the free energy change when 1 mol of ion is transferred from infinity in solution to the surface of the solid, was calculated from the K_{DR} value using Eq. (11) [63]:

$$E = \frac{1}{\sqrt{2K_{DR}}} \tag{11}$$

2.6. Adsorption kinetic studies

The kinetics of adsorption were studied to elucidate the mechanism of the adsorption process and the rate of Ni(II) uptake by the adsorbents. In the present study, the experimental kinetic data were analyzed using pseudo-first-order and pseudo-second-order models. Lagergren's pseudo-first-order [64] equation is written as (Eq. (12)):

$$\frac{dq_t}{dt} = k_1(q_e - q_t) \tag{12}$$

where k_1 is the pseudo-first-order rate constant (min^{-1}).

The integrated form of Eq. (12) can be expressed as shown in Eq. (13):

$$\ln(q_e - q_t) = \ln q_e - k_1 t \tag{13}$$

The k_1 and q_e can be calculated from the slope and intercept of the linear plot of $\ln(q_e - q_t)$ versus t, respectively.

The pseudo-second-order kinetic rate equation [65] based on equilibrium adsorption can be expressed by the following equation:

$$\frac{dq_t}{dt} = k_2(q_e - q_t)^2 \tag{14}$$

where k_2 [g/(mg min)] is the pseudo-second-order rate constant. The integrated form of Eq. (14) can be expressed as shown in Eq. (15):

$$\frac{t}{q_t} = \frac{1}{k_2 q_e^2} + \frac{1}{q_e}t \tag{15}$$

If the second-order kinetic model is applicable, the plot of t/q_t against t should give a linear relationship. The q_e and k_2 were obtained from the slope and intercept of the plot.

2.7. Error analysis

The best-fit mathematical model was selected based on error analysis. For this purpose, the chi-square (χ^2) test has been applied. If the data from the model are similar to the experimental data, χ^2 will be a small number, while if they differ, χ^2 will be a bigger number. Therefore, it is necessary to analyze the data set using the non-linear chi-square test to confirm the best-fit isotherm for the sorption system [6]. The chi-square can be calculated using Eq. (16):

$$\chi^2 = \sum_{i=1}^{N} \frac{\left(q_{e,calc} - q_{e,exp}\right)^2}{q_{e,calc}} \tag{16}$$

where $q_{e,exp}$, and $q_{e,calc}$ (mg/g) are the experimental and calculated amounts of Ni(II) adsorbed at equilibrium obtained from the experiment and mathematical model, respectively, and N is the number of data points.

3. Results and discussion

The physicochemical analysis shows that the WCS-Raw adsorbent contains 7.25 % moisture, 33.36 % volatile matter, 16 % ash, and 43.39 % fixed carbon. The bulk density and acid value of WCS-Raw were determined to be 0.922 g/cm^3 and 0.4 mEqH$^+$/g, respectively.

Scanning electron microscopy (SEM) images were employed to investigate the surface texture and morphology of the WCS-Raw, WCS-NaOH, WCS-CA, WCS-AM, and WCS-Si adsorbents. As observed from the SEM images in Fig. 1a–e, the adsorbents were porous and had irregular surface textures. The modified adsorbents had a higher surface roughness than WCS-Raw, while the WCS-Si

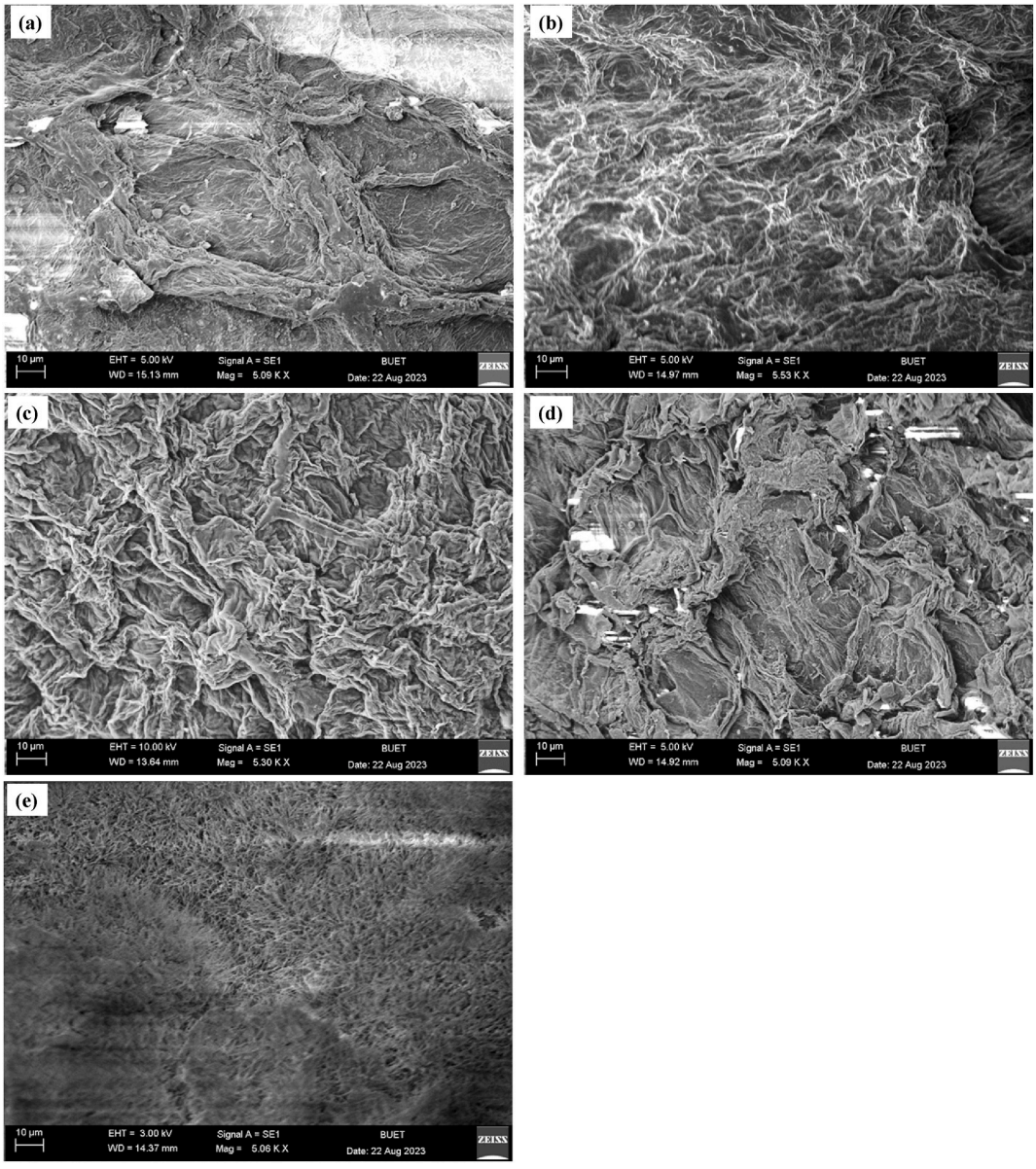

Fig. 1. Scanning electron micrograph: (a) WCS-Raw, (b) WCS-NaOH, (c) WCS-CA, (d) WCS-AM, and (e) WCS-Si

sample displayed a fiber-like structure.

The FTIR spectroscope was used to determine the presence of functional groups on the surface of adsorbents. The FTIR spectra of WCS-Raw and WCS-Si are shown in Fig. 2. As depicted from the spectrum of WCS-Raw (Fig. 2), the peak at 3385.07 cm^{-1} is due to O–H stretching [66], while the trough in the range of 3000–2850 cm^{-1} is due to the aliphatic C–H group [67–69]. A sharp P–H stretching peak is found at 2358.94 cm^{-1} [70]. The peaks at 1735.93 and 1635.23 cm^{-1} are attributed to the C═O stretching of the carboxyl group [71]. The absorption band at around 1240 cm^{-1} is assigned to $–SO_3$ stretching [72]. The peak at around 1051.20 cm^{-1} corresponds to alcohols or phenols, indicating the presence of polyphenols [73]. The stretching vibration of C–O or C–*O*–C in cellulose and hemicelluloses is observed at 1036∼1088 cm^{-1} [17]. The analysis revealed that the WCS-Raw sample contained functional groups such as OH, COOH, and SO_3H groups.

As observed from the FTIR spectrum of WCS-Si (Fig. 2), the broad absorption band in the 3700–3000 cm^{-1} spectral region can be assigned to the isolated and surface OH groups of Si–OH, whereas the absorption band at around 1630 cm^{-1} may be ascribed to bending vibration of O–H group of adsorbed H_2O molecule [74–77]. The absorption peaks at 1110 cm^{-1} and 966 cm^{-1} are due to the Si–O asymmetrical stretching vibration [76–78]. The O–Si–O stretching vibration was observed at 797 cm^{-1} [79]. The bending Si–*O*–Si modes can be ascribed to the bands at 619, 511.14, and 482.2 cm^{-1} [75,77,80].

The FTIR spectra of WCS-NaOH, WCS-CA, and WCS-AM were compared in Fig. 3. Having compared FTIR spectra for WCS-NaOH and WCS-CA, we found new peaks at 1602, 1718.5, and 1740 cm^{-1} in the FTIR spectrum of WCS-CA, which were characteristic of carbonyl group stretching in carboxylic acids and carbonyl groups [1,81–85]. The trough in the range of 2500–3400 cm^{-1} contains multiple peaks, which may be due to the OH group and C–H stretching vibration [1,86]. The peaks at 1032 and 1057 cm^{-1} indicate the stretching vibration of C–O groups attributed to carboxylic acid, alcoholic, phenolic, ether, and ester groups of lignin, cellulose, and hemicellulose components [87,88]. The OH group is responsible for the IR peak at 3655 cm^{-1} [89]. It indicates the introduction of the carboxylic acid group onto the WCS-NaOH as a result of treatment with citric acid.

In the FTIR spectra of WCS-AM, the peak at 1720 cm^{-1} may be due to the carbonyl group [1,81–83], and the peak at around 1037 cm^{-1} may be due to C–N stretching of the amine group [90] or the OH group of carbohydrate [91]. The 1699.2 cm^{-1} peak is linked to amide I [92–94], while the 2372 and 3715 cm^{-1} peaks are attributed to the hydroxyl and amine groups, respectively [95,96]. In addition, the vibration by the NH_2 band that appeared in the region 3200–3400 cm^{-1} is due to the grafting of acrylamide on WCS-NaOH [92]. Therefore, the acrylamide grafting was successful in the WCS-AM sample.

Fig. S1 shows the FTIR spectra of WCS-Raw, WCS-Si, WCS-CA, and WCS-AM, which were recorded after Ni(II) adsorption. The FTIR spectra obtained before and after adsorption of Ni(II) were compared, and the major changes in the spectra due to Ni(II) sorption are presented in Table S1. For WCS-Raw, the FTIR peaks appeared before adsorption at 3385.07, 1635.23, and 1051.20 cm^{-1} shifted to 3270.84, 1625.97, and 1028.97 cm^{-1}, respectively, after adsorption. In addition, the peaks at 1735.93 and 1240 cm^{-1} appeared before adsorption and almost disappeared after adsorption. For WCS-Si before adsorption, the FTIR peaks appeared at 3454.50, 1110, 796, 511.14, and 619 cm^{-1} which changed to 3372.7, 1028, 872, 564.42, and 600.62 cm^{-1}, respectively, after adsorption. New peaks were also observed at 421.44 and 405.56 cm^{-1} after adsorption. The peaks at 1032, 1057, and 1602 cm^{-1} in the FTIR spectrum of WCS-CA before adsorption changed to 1029.8, 1053.38, and 1633 cm^{-1} after adsorption. Additionally, the bands at 1718.5 and 3655 cm^{-1} almost disappeared after the adsorption of Ni(II) onto WCS-CA. The FTIR peaks at 1037, 1720, and 3239.42 cm^{-1} for WCS-AM before adsorption were found to shift at 1030.85, 1651.19, and 3334.58 cm^{-1} after adsorption. Moreover, the peaks at 2372 and 3715 cm^{-1}

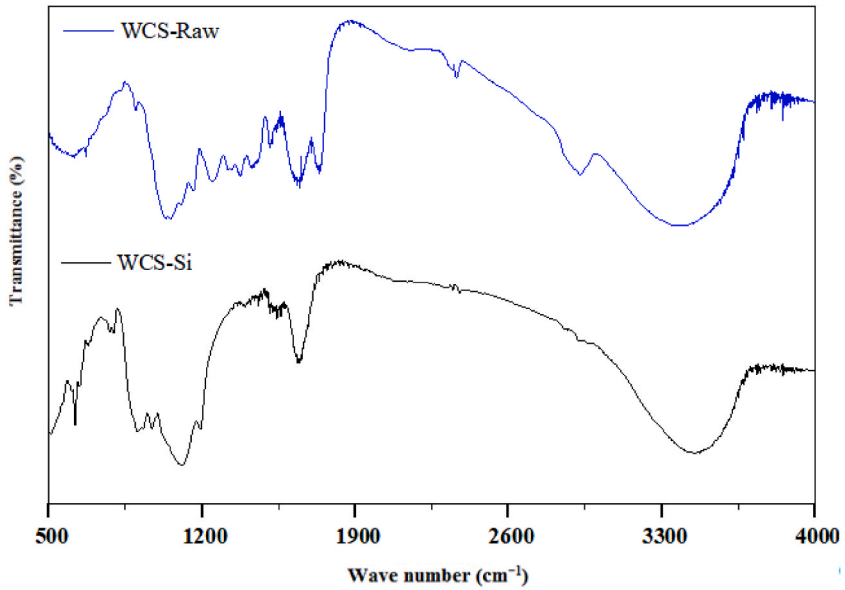

Fig. 2. FTIR spectra of WCS-Raw and WCS-Si

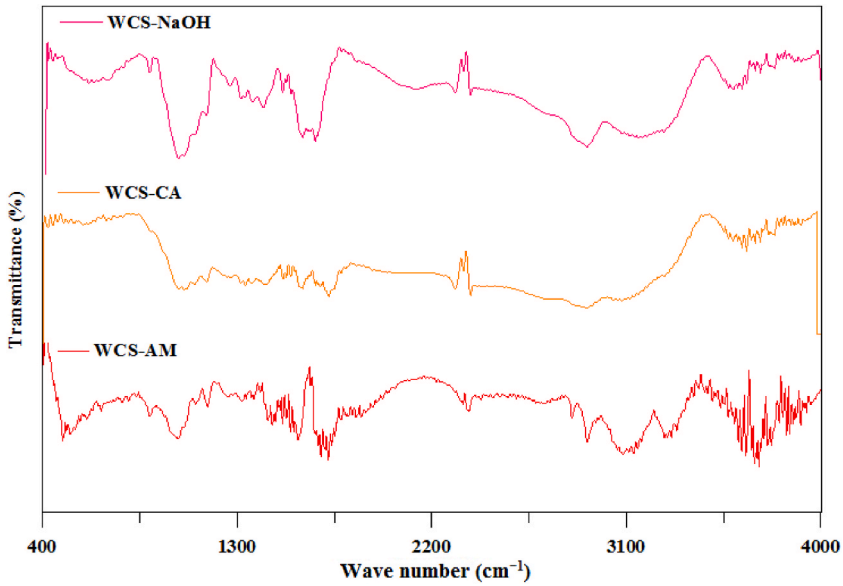

Fig. 3. FTIR spectra of WCS-NaOH, WCS-CA, and WCS-AM.

disappeared after adsorption. The observation suggests that the disappearance, shifting, and emergence of new peaks indicate the adsorption of Ni(II) onto the adsorbents.

The textural property of the raw and modified WCS adsorbents was investigated by N_2 sorption measurement at liquid N_2 temperature. For WCS-Raw, WCS-CA, WCS-AM, and WCS-Si, the N_2 adsorption-desorption isotherms, and the corresponding BJH pore size distribution curves are shown in Figs. 4 and 5, respectively.

According to the IUPAC classification, all four adsorbent samples exhibit type II isotherm and type H3 hysteresis loop (Fig. 4) [97]. The Type II isotherm illustrates unrestricted monolayer-multilayer adsorption [98]. The H3 type hysteresis loop is a characteristic of solids consisting of aggregates or agglomerates of particles forming slit-shaped pores (plates or edged particles like cubes), with nonuniform size and/or shape [99]. The BET surface area (S_{BET}), total pore volume, and pore size of the four samples are summarized in Table 1. As shown in Table 1, S_{BET} values are almost the same for WCS-Raw, WCS-CA, and WCS-AM. Among the four samples, the WCS-Si adsorbent has the highest surface area (3.55 m^2/g), specific pore volume (0.0198 cm^3/g), and average pore diameter (20.58 nm). Fig. 5 reveals that WCS-Si has a broader distribution of pore size, in the region 1.9 nm–45 nm (mesoporous range: 2–50 nm), whereas the other three samples have a narrow distribution of pore size, mostly found in the range of 2–7 nm.

Fig. 6 shows that the pHpzc of WCS-Raw, WCS-CA, WCS-AM, and WCS-Si are 5.62, 4.05, 4.2, and 9.55, respectively. At pH $<$ pHpzc, the WCS adsorbent surface is charged positively, while at pH $>$ pHpzc, the surface is negatively charged and will favor the adsorption of cationic species.

Fig. 7 shows the influence of adsorbent doses on Ni(II) sorption onto WCS-Raw, WCS-CA, WCS-AM, and WCS-Si. For all four

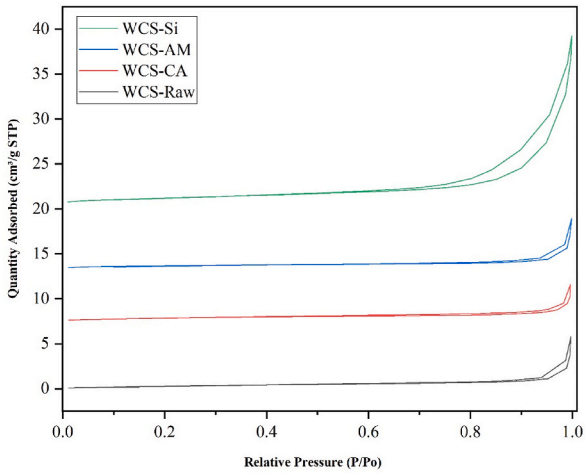

Fig. 4. Nitrogen adsorption-desorption isotherms of WCS-Raw, WCS-CA, WCS-AM, and WCS-Si

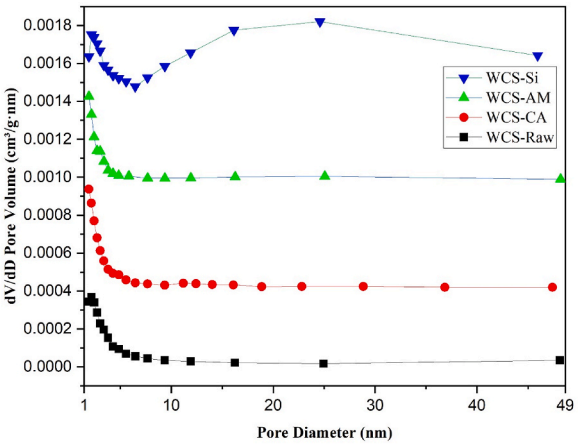

Fig. 5. Pore size distribution curves of WCS-Raw, WCS-CA, WCS-AM, and WCS-Si

Table 1
Nitrogen sorption porosimetry studies[a] of adsorbents.

Adsorbent	*S*BET (m^2/g)	Pore size (nm)	Pore volume (cm^3/g)
WCS-Raw	1.23	16.55	0.0035
WCS-CA	1.28	12.64	0.0029
WCS-AM	1.22	12.98	0.0035
WCS-Si	3.55	20.58	0.0198

[a] Surface areas were determined by BET, pore diameters by BJH theory (applied to the adsorption branch), and pore volumes by single-point analysis.

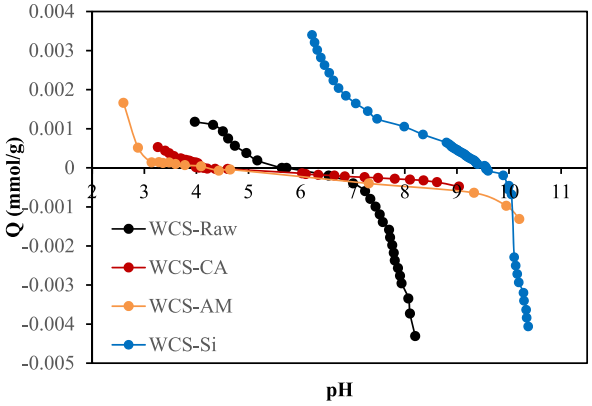

Fig. 6. Surface charge Q of WCS-Raw, WCS-CA, WCS-AM, and WCS-Si as a function of pH.

adsorbents, adsorption density declined with the increase in adsorbent dosage. It might be due to the split in the flux or the concentration gradient between the Ni(II) concentration in the solution and the Ni(II) concentration on the surface of biosorbents [100].

Ni(II) exists in aqueous solutions as a positively charged species. The surface charge on the adsorbent, which is influenced by the solution pH, has the greatest effect on Ni(II) uptake. The effect of the initial solution pH (3–7.5) on the adsorption of nickel ions onto WCS-Raw, WCS-CA, WCS-AM, and WCS-Si adsorbents was studied, and the results are presented in Fig. 8.

As shown in Fig. 8, the biosorption capacities of Ni(II) onto the four adsorbents were smaller at low pH, and the adsorption was favorable at pH 7–7.5. The decreased adsorption density at lower pH could be attributed to the repulsive force developed between the positively charged adsorbent surface (at pH < pHpzc) and Ni(II) cation, as well as to the stiff competition faced by Ni(II) cation from the greater number of available hydrogen ions for vacant adsorption sites on the adsorbents.

At pH > pHpzc, the adsorbent surface is negatively charged and will favor the adsorption of cationic species by electrostatic attraction [101]. Consequently, the adsorption capacities of WCS-Raw, WCS-CA, and WCS-AM increased with the increase in pH of the initial solution. Similar observations were reported for the sorption of Ni(II) onto lignocellulose/montmorillonite nanocomposite [5], activated carbon and sawdust [22,102].

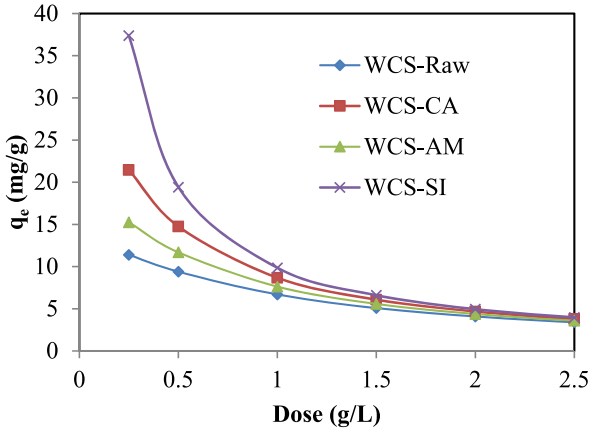

Fig. 7. Effect of adsorbent dose on the sorption of Ni(II) onto WCS-Raw, WCS-CA, WCS-AM, and WCS-Si (pH = 7; C_0 = 10 mg/L; V = 200 mL; dose = 0.25–2.5 g/L; t = 12 h).

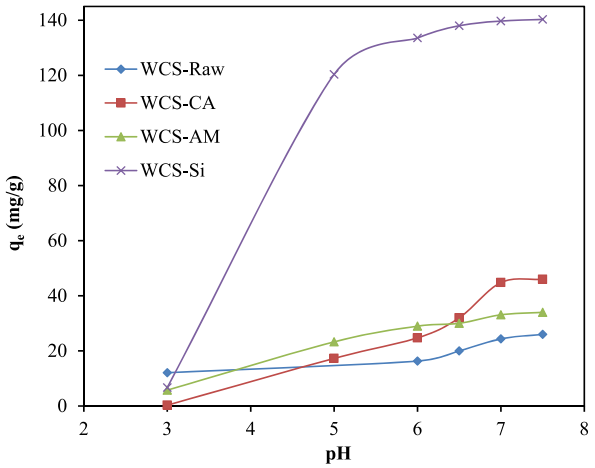

Fig. 8. Effect of pH on the adsorption of Ni(II) onto WCS-Raw, WCS-CA, WCS-AM, and WCS-Si (pH = 3–7.5; C_0 = 57.89, 56.17, 56.17, 58.29 mg/L for WCS-Raw, WCS-CA, WCS-AM, and WCS-Si, respectively; V = 200 mL; W = 0.05 g; t = 12 h).

The adsorption of Ni(II) ions on WCS-Si, however, was found to occur at pH < pHpzc, indicating that non-electrostatic interaction may be responsible for this adsorption. Similar results have been reported for the adsorption of Cu(II) onto ZnO nanoparticles [103] and Cd onto orange peel-derived biochar [104]. Subsequent experiments were conducted at pH 7 due to the potential for metal

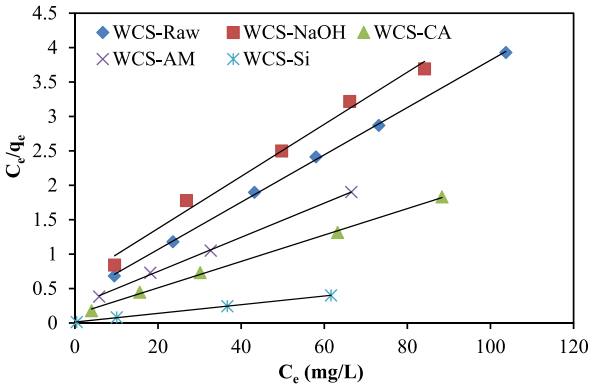

Fig. 9. Langmuir isotherm plots for Ni(II) sorption onto WCS-Raw, WCS-CA, WCS-AM, WCS-Si, and WCS-NaOH (C_0 = 10–130 mg/L; pH = 7; V = 200 mL; W = 0.05 g; t = 12 h).

hydroxide precipitation at higher pH levels [102].

3.1. Adsorption isotherm study

The adsorption equilibrium data of Ni(II) sorption onto various WCS-based adsorbents were fitted to Langmuir (Eq. (5)), Freundlich (Eq. (6)), and Elovich isotherm (Eq. (7)) models as shown, respectively, in Figs. 9–11. The isotherm parameters, correlation coefficient (R^2), and error function (Chi-square (χ^2)) were summarized in Table 2. As shown in Table 2, the Langmuir model shows the highest correlation coefficient and the lowest Chi-square values for WCS-Raw, WCS-CA, WCS-AM, and WCS-Si adsorbents, which suggests the best fitting of experimental equilibrium data by this model. The values of maximum monolayer sorption capacity (q_m) calculated from the Langmuir model were 29.06, 52.08, 40.32, and 158.73 mg/g for WCS-Raw, WCS-CA, WCS-AM, and WCS-Si, respectively. The highest sorption capacity of WCS-Si is consistent with its greatest surface area. A greater surface area might contain more active sites, contact areas, and surface functional groups suitable for adsorption [17]. Although the R^2 value of the Freundlich model is higher than that of the Langmuir model in the case of WCS-NaOH adsorbent, a value of 0.3232 for 1/n as calculated from the Freundlich isotherm equation indicates that the normal Langmuir isotherm model is suitable for describing the adsorption equilibrium data [59].

From Tables 2 and it was also observed that the Langmuir maximum adsorption capacity of WCS-NaOH was almost similar to that of WCS-Raw. Therefore, the improved adsorption capacity of WCS-AM and WCS-CA adsorbents was due to the insertion of active functional groups on the surface of the WCS-NaOH adsorbent.

The separation factor (R_L) was used to predict whether the adsorption process might be irreversible ($R_L = 0$), favorable ($0 < R_L < 1$), or unfavorable ($R_L > 1$), and was estimated by the following equation (Eq. (17): [105]:

$$R_L = \frac{1}{1 + K_L C_0} \tag{17}$$

where K_L is the Langmuir constant and C_o is the highest initial solution concentration of Ni(II) used in an equilibrium adsorption study.

The values of R_L (Table 2) were in the range of 0.02–0.18, which indicated that the adsorption of NI(II) was favorable for all the prepared adsorbents.

The nonlinear plots of q_e versus C_e for the Langmuir, Freundlich, and Elovich isotherm models are shown in Fig. S2. The experimental equilibrium results were more accurately predicted by the Langmuir model than by the Freuindlich and Elovich isotherm models, as evidenced in Fig. S2.

The equilibrium data were also treated with the D-R isotherm model to find out the adsorption mechanism. The value of the mean free energy of adsorption (E) estimated from the D-R isotherm model (Fig. 12) provides information about the nature of biosorption. The predominant mechanism is physical when $1 < E < 8$ KJ/mol, chemical when $E > 16$ kJ/mol, and ion exchange when $8 < E < 16$ kJ/mol [6,49,106]. As shown in Table S2, the values E for WCS-Raw, WCS-NaOH, WCS-CA, WCS-AM, and WCS-Si were estimated to be 15.8, 12.9, 15.8, 12.9, and 15.8 kJ/mol, respectively, suggesting the predominance of ion exchange process.

The maximum adsorption capacity (q_m) of several adsorbents for the uptake of Ni(II) from aqueous solutions is listed in Table 3.

It is obvious from Table 3 that WCS and modified WCS adsorbents in this study have significantly higher adsorption capacities than the others. The above-mentioned results imply that the WCS-based adsorbents are excellent candidates for the removal of Ni(II) from wastewater.

3.2. Adsorption kinetic study

Contact time between the adsorbent and adsorbate has a significant impact on the adsorption process. Fig. 13 illustrates the amount of Ni(II) adsorption onto WCS-Raw, WCS-CA, WCS-AM, and WCS-Si adsorbents as a function of contact time. It is observed that the uptake of Ni(II) is rapid during the initial stage (first 20 min), and after that, the rate decreases gradually, leading to equilibrium. The rapid increase of q_t during the initial period may be due to a greater number of unoccupied adsorption sites on the surface of

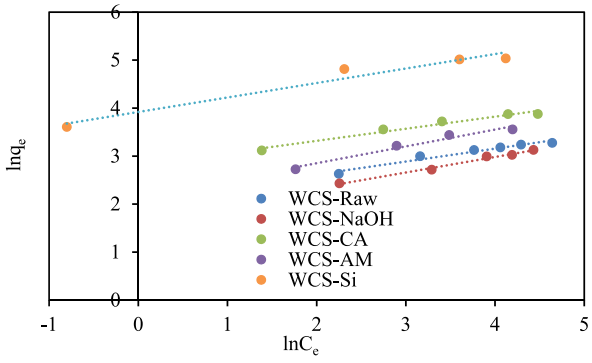

Fig. 10. Freundlich isotherm plots for Ni(II) sorption onto WCS-Raw, WCS-CA, WCS-AM, WCS-Si, and WCS-NaOH (C_0 = 10–130 mg/L; pH = 7; V = 200 mL; W = 0.05 g; t = 12 h).

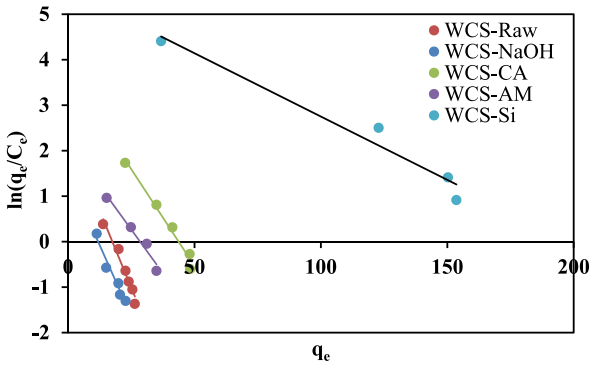

Fig. 11. Elovich isotherm plots for Ni(II) sorption onto WCS-Raw, WCS-CA, WCS-AM, WCS-Si, and WCS-NaOH (C_0 = 10–130 mg/L; pH = 7; V = 200 mL; W = 0.05 g; t = 12 h).

Table 2
Langmuir, Freundlich, Elovich isotherm parameters, correlation coefficient, and chi-square for the adsorption of Ni(II) on different adsorbents.

	Type of adsorbent				
Parameter	WCS-Raw	WCS-NaOH	WCS-CA	WCS-AM	WCS-Si
Langmuir isotherm					
q_m (mg/g)	29.06	26.46	52.08	40.32	158.73
k_L (L/mg)	0.090	0.061	0.151	0.098	0.470
R^2	0.9994	0.9882	0.9987	0.9991	0.9995
R_L	0.1	0.18	0.062	0.119	0.021
χ^2	0.035	0.413	0.590	0.061	3.540
Freundlich isotherm					
n	3.721	3.095	3.969	2.853	3.314
k_F (mg/g)/(mg/L)$^{1/n}$	8.0125	5.4141	16.6915	8.595	50.38
R^2	0.9598	0.9890	0.9713	0.9677	0.9571
χ^2	0.232	0.063	0.448	0.378	7.409
Elovich isotherm					
q_{mE} (mg/g)	7.37	8.01	11.75	13.04	35.84
K_E (L/mg)	1.4581	0.5504	3.5151	0.6803	7.0736
R^2	0.9634	0.9576	0.9774	0.9635	0.9606
χ^2	1.598	0.953	3480	1.566	37.961

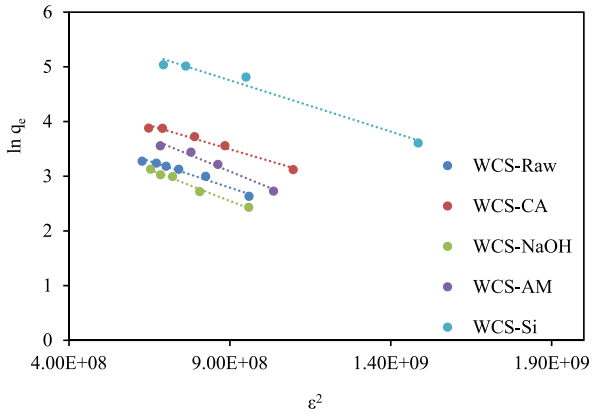

Fig. 12. D–R isotherm plots for Ni(II) sorption onto WCS-Raw, WCS-CA, WCS-AM, WCS-Si, and WCS-NaOH (C_0 = 10–130 mg/L; pH = 7; V = 200 mL; W = 0.05 g; t = 12 h).

adsorbents. The slower adsorption at the later stage may be due to the decrease in the number of active sites available on the adsorbents [1,34].

The experimental kinetic data of Ni(II) adsorption onto four adsorbents (WCS-Raw, WCS-CA, WCS-AM, and WCS-Si) were fitted to the pseudo-first-order and the pseudo-second-order models, as illustrated in Figs. 14 and 15. The model parameters, the values of correlation coefficient (R^2), calculated equilibrium adsorption density ($q_{e,calc}$), and chi-square (χ^2) are presented in Table 4. The

Table 3
Adsorption capacity of different adsorbents for Ni(II) adsorption.

Adsorbent [Reference]	Adsorption capacity *qm* (mg/g)
Malatya clay [107]	10.267
Sepiolite [108]	250
Citric acid-functionalized aloe vera leaf powder [19]	48.65
Chloroxylon swietenia activated carbon [109]	50.074
Na_2CO_3-modified steam-heated Aloe vera leaf powder [33]	28.99
Lemon peel [35]	7.4
Cassava peel [35]	6.4
Raw mahogany sawdust [110]	5.35
Formaldehyde-treated mahogany sawdust [110]	13.42
Magnetic chitosan beads [111]	0.064
Aloe barbadensis Miller leaves [34]	10
Tea waste [36]	14.09
Activated carbons from doum-pulm-seed [6]	13.51
Activated carbon from sugar cane [102]	27.57
Blue-green marine algae [20]	42.05
Nano alumina [8]	30.82
Chitin micro-particles [112]	42.62
Activated carbons from scrap tire [113]	25
Charcoal ash [114]	10.86
*Ceibapentandra*hulls [16]	34.34
Lignin [115]	5.99
Rice straw [37]	35.08
Barley straw [116]	35.8
Calcinedphosphate [117]	15.53
Red mud [117]	13.69
Clarified sludge [117]	14.30
Magnetosome [11]	2.08
WCS-RAW	29.07
WCS-CA	52.08
WCS-AM	40.32
WCS-Si	158.7

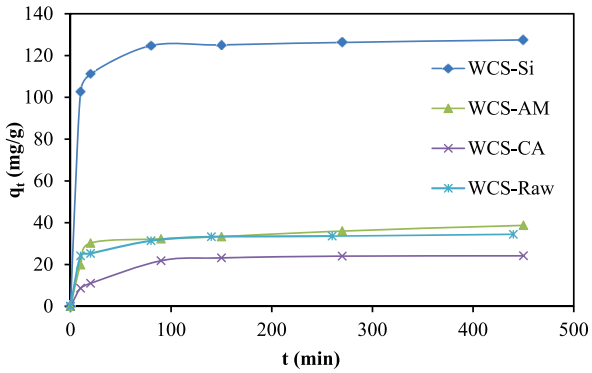

Fig. 13. Effect of contact time on the adsorption capacity for Ni(II) sorption onto WCS-Raw, WCS-CA, WCS-AM, and WCS-Si adsorbents (C_0 = 50.94 mg/L for WCS-Raw and 54.78 mg/L for WCS-CA, WCS-AM, and WCS-Si); pH = 7; V = 200 mL; W = 0.05 g; t = 0–540 min).

pseudo-second-order model had higher R^2 values and lower Chi-square values than the pseudo-first-order model (Table 4). Fig. (S3) compares the experimental kinetic data to the fitted data calculated from the pseudo-first-order model and the pseudo-second-order model. It is clear from Fig. (S3) that the q_t values calculated from the pseudo-first-order model did not agree with the experimental q_t values. On the other hand, the pseudo-second-order kinetic model showed a strong fit to the kinetic data. Based on these results, it can be concluded that the pseudo-second-order kinetic model, which predominantly referred to chemisorption processes and the interaction of functional groups on adsorbents with contaminants, provided a good correlation in contrast to the pseudo-first-order model for the sorption of Ni(II) in the present study.

3.3. Thermodynamic study

Thermodynamic behavior of Ni(II) sorption onto WCS-Raw, WCS-CA, WCS-AM, and WCS-Si was revealed by evaluating thermodynamic parameters such as change in Gibbs free energy (ΔG^o, kJ/mol), enthalpy (ΔH^o, kJ/mol), and entropy (ΔS^o, J/mol K) using the

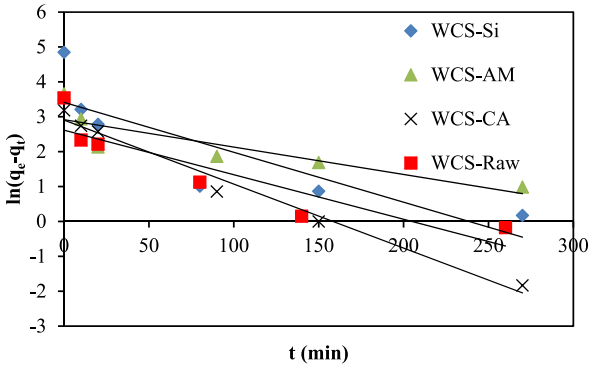

Fig. 14. Pseudo-first order kinetics for the adsorption of Ni(II) onto WCS-Raw, WCS-CA, WCS-AM, and WCS-Si adsorbents.

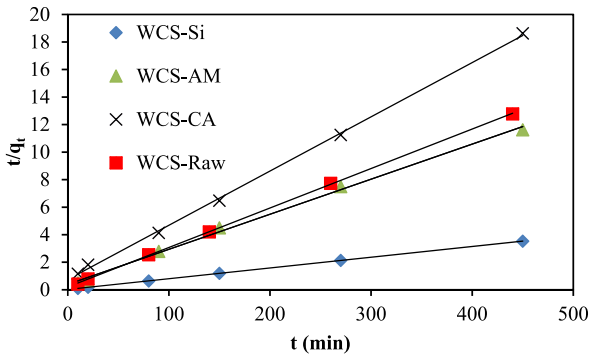

Fig. 15. Pseudo-second order kinetics for the adsorption of Ni(II) on WCS-Raw, WCS-CA, WCS-AM, and WCS-Si adsorbents.

Table 4
Pseudo-first-order and pseudo-second-order kinetics parameters for Ni(II) sorption onto WCS-Raw, WCS-CA, WCS-AM, and WCS-Si adsorbents.

			Pseudo-first-order				Pseudo-second-order			
	C_0 (mg/g)	$q_{e,exp}$ (mg/g)	k_1 (min^{-1})	$q_{e,calc}$ (mg/g)	R^2	χ^2	k_2 (gmg^1min^{-1})	$q_{e,calc}$ (mg/g)	χ^2	R^2
WCS-Raw	50.94	34.44	0.0128	13.68	0.816	31.5	0.00401	34.84	0.004	0.999
WCS-CA	54.78	24.16	0.0183	18.28	0.983	1.8	0.00209	25.38	0.058	0.999
WCS-AM	54.78	38.72	0.0078	18.48	0.754	22.1	0.00167	39.22	0.006	0.997
WCS-Si	54.78	127.5	0.014	30.36	0.724	310	0.00278	125	0.05	1

Table 5
Thermodynamic parameters for the sorption of Ni(II) onto WCS-Raw, WCS-CA, WCS-AM, and WCS-Si

Adsorbent	T (K)	ΔG^o (kJ/mol)	ΔS^o (J/(mol K))	ΔH^o (kJ/mol)
	313.15	−4.13799		
WCS-Raw	298.15	−1.87222	78.9963	20.88061
	291.15	−2.63941		
	313.15	−2.96699		
WCS-CA	301.15	−2.67181	32.5385	7.190945
	291.15	−2.24997		
	313.15	−1.56521		
WCS-AM	301.15	−1.30693	32.89018	8.688961
	291.15	−0.83996		
	323.15	−13.4196		
WCS-Si	313.15	−9.56271	279.2423	77.26699
	291.15	−4.19999		

following equations [118] (Eq. (18)–(20)) and the results are presented in Table 5:

$$\Delta G^o = -RT\ln K_d \tag{18}$$

$$\ln K_d = \frac{\Delta S^o}{R} - \frac{\Delta H^o}{RT} \tag{19}$$

where R (8.314 J mol^{-1} K^{-1}) is the universal gas constant, T (K) is the absolute solution temperature and K_d is the distribution coefficient defined as:

$$K_d = \frac{q_e}{C_e}. \tag{20}$$

The values of ΔH^o and ΔS^o were calculated from the slope and intercept of the linear plot of $\ln K_d$ versus $1/T$ (Fig. 16) for an initial Ni(II) concentration of 19.5 mg/L.

The negative values of ΔG^o (Table 5) at different temperatures indicate the feasibility and spontaneity of the adsorption process [119]. The positive values of ΔS^o reflect the affinity of the adsorbents for the Ni(II) ions and the higher disorder of the adsorption system [34]. The positive values of ΔH^o suggest the endothermic nature of Ni(II) adsorption onto the adsorbents [27]. A similar result was reported for the adsorption of Cr(VI) on cerium phosphate polypyrrole [119].

3.4. Desorption and regeneration

To explore the potentiality of recovery of nickel ions and reusability of the as-prepared adsorbents in the present study, desorption experiments were carried out. For each type of adsorbent, an adsorption equilibrium experiment was first conducted at pH 7, and the adsorbent was then separated from the adsorption system by centrifugation and dried in air. Thereafter, desorption was performed by contacting the nickel-ion-loaded adsorbent with 200 mL of distilled water adjusted to pH 2.5. After desorption, the sample was centrifuged, and the concentration of Ni ions in the supernatant solution was measured.

The percentage recovery was calculated using the following equation (Eq. (21)):

$$\%\ Recovery = 100 \times \frac{Amount\ of\ Ni(II)\ ion\ desorbed}{Amount\ of\ Ni(II)\ ion\ adsorbed} \tag{21}$$

Fig. 17 shows the adsorption and desorption potential of Ni(II) by WCS adsorbents in three consecutive cycles. As shown in the figure, the adsorption percentage remained almost consistent across three consecutive cycles. In the third cycle, 80–93 % of the adsorbed Ni(II) could be desorbed from the adsorbents by the swing of the solution pH to 2.5. At low pH, the desorption of positively charged metal ions should be facilitated by electrostatic repulsion due to the rise in positively charged species. Therefore, the WCS adsorbents in this study can be easily reused for nickel adsorption and recovery.

3.5. Adsorption mechanism

Various active sites, such as carboxyl, amide, and silanol groups, are responsible for Ni(II) adsorption. At pH > 4, the carboxyl groups are deprotonated and exist as the negatively charged carboxylate ($-COO^-$) form [22]. Consequently, adsorption may occur by ion exchange and electrostatic attraction between the negatively charged carboxylate group and the Ni(II) cation (Eq. (22) and Eq. (23)):

$$(WCS) - (COOH)_2 = (WCS) - (COO^-)_2 + 2H^+ \tag{22}$$

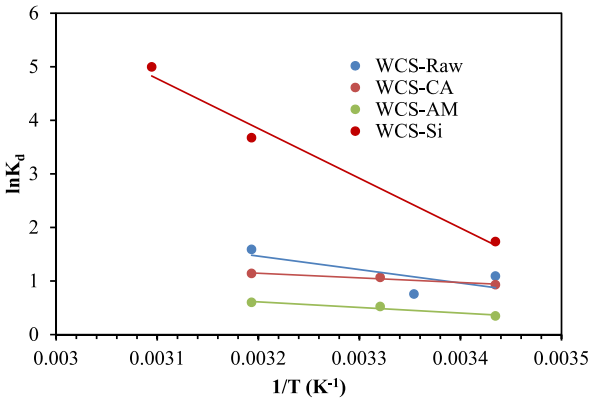

Fig. 16. Plot of $\ln K_d$ versus 1/T for Ni(II) sorption onto WCS-Raw, WCS-CA, WCS-AM, and WCS-Si (C_0 = 19.5 mg/L; pH = 7; V = 200 mL; W = 0.05 g; t = 12 h).

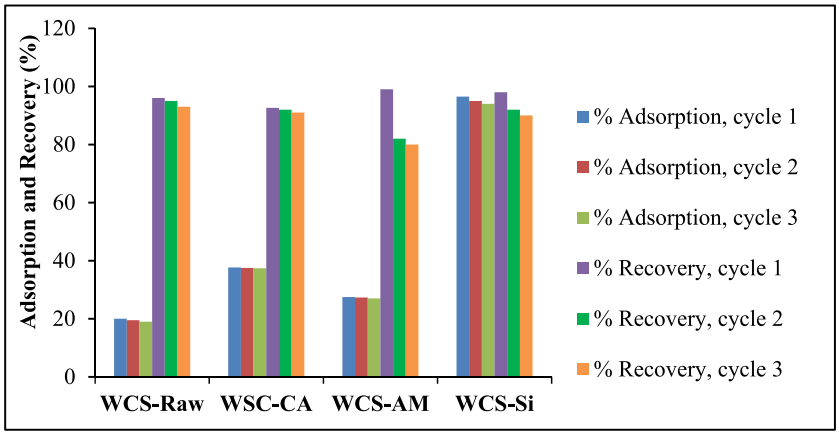

Fig. 17. Adsorption and recovery of Ni(II) ions for WCS-Raw, WCS-CA, WCS-AM, and WCS-Si adsorbents (Co = 25 mg/L (for WCS-Raw, WCS-CA and WCS-AM) and 24.53 mg/L (for WCS-Si); V = 200 mL; W = 0.05 g; pH = 7).

$$(\boldsymbol{WCS})-(\boldsymbol{COO^-})_2+\boldsymbol{Ni^{2+}}=(\boldsymbol{WCS})-(\boldsymbol{COO^-})_2\boldsymbol{Ni^{2+}} \tag{23}$$

Adsorption on the amide group may happen by complexation between the amide group and nickel cation [120]. Li et al. [121] reported the binding of lead ions by the amide group through electrostatic attraction or complexation. The EDX analysis (Fig. S4 and Table S3) shows the presence of 21.70 % Si and 44.47 % O atoms in the WCS-Si sample. In an aqueous solution, the oxide of silicon contains silanol (≡Si–OH) groups and adsorption may happen via cation exchange with the protons from silanol groups [122–124] as shown in Eq. (24):

$$\mathbf{2}(\equiv \text{Si–OH})+\boldsymbol{Ni^{2+}}=(\equiv \boldsymbol{SiO^-})_2\boldsymbol{Ni^{2+}}+\mathbf{2}\boldsymbol{H^+} \tag{24}$$

The adsorption of NI(II) on carboxyl, amide, and silanol groups has been schematically presented in schemes S1, S2, and S3., respectively.

3.6. Cost estimation

Cost estimation is an important aspect of selecting the suitable adsorbent for the removal of heavy metal from wastewater. The cost of adsorbent per gram of adsorbate was calculated using Eq. (25) [125]:

$$\boldsymbol{Adsorption\ cost}\left(\frac{\boldsymbol{USD}}{\boldsymbol{g\ adsorbate}}\right)=\frac{\left[\boldsymbol{Chemical\ Purchase\ cost}\left(\frac{\boldsymbol{USD}}{\boldsymbol{g}}\right)+\boldsymbol{Energy\ cost}\left(\frac{\boldsymbol{USD}}{\boldsymbol{g}}\right)\right]}{\boldsymbol{Adsorption\ capacity}\left(\frac{\boldsymbol{mg}}{\boldsymbol{g}}\right)\times\mathbf{10}^{-3}\ \frac{\boldsymbol{g}}{\boldsymbol{mg}}} \tag{25}$$

Water caltrop epicarp (WCS), a waste biomass in Bangladesh, was obtained free of charge from a local fruit processing industry (in Sylhet district, Bangladesh). The expense for chemicals was obtained from budgeting chemical quotations provided by suppliers. The cost of electrical energy was estimated using electricity pricing from a local electricity company (Bangladesh Power Development Board (BPDB), Sylhet). The major pieces of power-consuming equipment were an electric furnace, magnetic stirrer, and drying oven. The cost of adsorbent per gram of adsorbed Ni(II) was calculated to be 0.0223, 0.02625, 0.01778, 0.13779, and 0.00525 $/g for WCS-Raw, WCS-NaOH, WCS-CA, WCS-AM, and WCS-Si, respectively. Additionally, prices will decrease because of its strong ability to regenerate. The produced WCS materials can be used as adsorbents for low-cost environmental pollution remediation.

4. Conclusion

Nickel is a transition metal with a wide environmental distribution. Three modified WCS-based adsorbents, such as WCS-CA, WCS-AM, and WCS-Si, were successfully prepared from WCS and used for the adsorption of nickel ions from aqueous solutions. The results showed that factors like adsorbent dosage, pH, initial Ni(II) concentration, and contact time significantly affect Ni(II) adsorption. FTIR analysis confirmed the successful introduction of citric acid and acrylamide onto the surface of WCS and the sorption of Ni (II) onto the adsorbents. The adsorption capacity increased with the increase in solution pH, and the optimal pH value was 7. Adsorption density increases rapidly during the initial contact period, then gradually reaches equilibrium. The adsorption followed pseudo-second-order kinetics and the Langmuir isotherm model. The modified WCS adsorbents had greater biosorption capacities for Ni(II) than the un-modified adsorbent (WCS-Raw). The maximum adsorption capacity (q_m) of WCS-Raw was 29.06 mg/g, while that of the modified adsorbents such as WCS-CA, WCS-AM, and WCS-Si was 52.08, 40.32, and 158.73 mg/g, respectively. The thermodynamic analysis shows that the adsorption process was endothermic, spontaneous, and feasible. For WCS-Raw, WCS-CA, WCS-AM, and WCS-Si, the cost

of adsorbent per gram of adsorbed Ni(II) was calculated to be 0.0223, 0.01778, 0.13779, and 0.00525 $/g, respectively. The reusability study indicates the excellent recycling capabilities of the adsorbents. Therefore, WCS and modified WCS adsorbents are promising for removing Ni(II) from wastewater, offering an excellent approach to handling agricultural biomass like WCS.

Data availability

Data will be made available on request.

CRediT authorship contribution statement

Muhammad Zobayer Bin Mukhlish: Writing – original draft, Validation, Supervision, Project administration, Methodology, Funding acquisition, Formal analysis, Conceptualization. **Shekh Nazibunnesa:** Formal analysis, Data curation, Conceptualization. **Shariful Islam:** Formal analysis, Data curation, Conceptualization. **Abu Saleh Al Mahmood:** Formal analysis, Data curation. **Md Tamez Uddin:** Writing – review & editing, Visualization.

Declaration of competing interest

The authors declare that they have no known competing financial interests or personal relationships that could have appeared to influence the work reported in this paper.

Acknowledgments

The authors wish to express great appreciation to the Center of Excellence, Shahjalal University of Science and Technology, Sylhet 3114, Bangladesh, for instrument support. The authors acknowledge the significant contributions of Md. Mehedi Hasan (Department of Chemical Engineering and Polymer Science, Shahjalal University of Science and Technology, Sylhet 3114, Bangladesh), including his extensive experiments in thermodynamic and recyclability studies.

Appendix A. Supplementary data

Supplementary data to this article can be found online at https://doi.org/10.1016/j.heliyon.2023.e21862.

References

[1] F. Mashkoor, A. Nasar, Inamuddin, A.M. Asiri, Exploring the reusability of synthetically contaminated wastewater containing crystal violet dye using tectona grandis sawdust as a very low-cost adsorbent, Sci. Rep. 8 (1) (2018) 8314.
[2] R. Baby, B. Saifullah, M.Z. Hussein, Palm Kernel Shell as an effective adsorbent for the treatment of heavy metal contaminated water, Sci. Rep. 9 (1) (2019), 18955.
[3] A.E. Burakov, et al., Adsorption of heavy metals on conventional and nanostructured materials for wastewater treatment purposes: a review, Ecotoxicol. Environ. Saf. 148 (2018) 702–712.
[4] A. Inyinbor Adejumoke, O. Adebesin Babatunde, P. Oluyori Abimbola, A. Adelani Akande Tabitha, O. Dada Adewumi, A. Oreofe Toyin, Water pollution: effects, prevention, and climatic impact, Water Chall. Urban. World 33 (2018) 33–47.
[5] X. Zhang, X. Wang, Adsorption and desorption of nickel (II) ions from aqueous solution by a lignocellulose/montmorillonite nanocomposite, PLoS One 10 (2) (2015), e0117077.
[6] M. El-Sadaawy, O. Abdelwahab, Adsorptive removal of nickel from aqueous solutions by activated carbons from doum seed (Hyphaenethebaica) coat, Alex. Eng. J. 53 (2) (2014) 399–408.
[7] U. EPA, Guidelines for Water Reuse. EPA/625/R-04/108, Camp Dresser and McKee Inc. for the US Environmental Protection Agency, 2004.
[8] V. Srivastava, C.H. Weng, V.K. Singh, Y.C. Sharma, Adsorption of nickel ions from aqueous solutions by nano alumina: kinetic, mass transfer, and equilibrium studies, J. Chem. Eng. Data 56 (4) (Apr. 2011) 1414–1422, https://doi.org/10.1021/je101152b.
[9] M.R. Awual, et al., Ligand based sustainable composite material for sensitive nickel (II) capturing in aqueous media, J. Environ. Chem. Eng. 8 (1) (2020), 103591.
[10] G. Genchi, A. Carocci, G. Lauria, M.S. Sinicropi, A. Catalano, Nickel: human health and environmental toxicology, Int. J. Environ. Res. Publ. Health 17 (3) (2020) 679.
[11] J.J. Jacob, R. Varalakshmi, S. Gargi, M.A. Jayasri, K. Suthindhiran, Removal of Cr (III) and Ni (II) from tannery effluent using calcium carbonate coated bacterial magnetosomes, NPJ Clean Water 1 (1) (2018) 1.
[12] E. Remoudaki, A. Hatzikioseyian, P. Kousi, M. Tsezos, The mechanism of metals precipitation by biologically generated alkalinity in biofilm reactors, Water Res. 37 (16) (2003) 3843–3854.
[13] Y.C. Sharma, V. Srivastava, S.N. Upadhyay, C.H. Weng, Alumina nanoparticles for the removal of Ni(II) from aqueous solutions, Ind. Eng. Chem. Res. 47 (21) (Nov. 2008) 8095–8100, https://doi.org/10.1021/ie800831v.
[14] A.H. Elshazly, A.H. Konsowa, Removal of nickel ions from wastewater using a cation-exchange resin in a batch-stirred tank reactor, Desalination 158 (1–3) (2003) 189–193.
[15] F. Akbal, S. Camcı, Copper, chromium and nickel removal from metal plating wastewater by electrocoagulation, Desalination 269 (1–3) (2011) 214–222.
[16] D.K.V. Ramana, D.H.K. Reddy, B.N. Kumar, Y. Harinath, K. Seshaiah, Removal of nickel from aqueous solutions by citric acid modified *Ceiba pentandra* hulls: equilibrium and kinetic studies, Can. J. Chem. Eng. 90 (1) (Feb. 2012) 111–119, https://doi.org/10.1002/cjce.20565.
[17] S. Wang, N. Wang, K. Yao, Characterization and interpretation of Cd (II) adsorption by different modified Rice straws under contrasting conditions, Sci. Rep. 9 (2019), 17868.

[18] K. Santhy, P. Selvapathy, Removal of heavy metals from wastewater by adsorption on coir pith activated carbon, Separ. Sci. Technol. 39 (14) (Nov. 2004) 3331–3351, https://doi.org/10.1081/SS-200036561.

[19] W.A. Al-Amrani, R. Abdullah, M.A.K. Megat Hanafiah, F.B.M. Suah, Removal of Ni (II) ions by citric acid-functionalised aloe vera leaf powder-characterisation, kinetics, and isotherm studies, J. Ecol. Eng. 24 (4) (2023). Accessed: Sep. 27, 2023. [Online]. Available: http://www.jeeng.net/pdf-159633-87955?filename=Removal%20of%20Ni_II_%20Ions%20by.pdf.

[20] R. Ramadoss, D. Subramaniam, Removal of divalent nickel from aqueous solution using blue-green marine algae: adsorption modeling and applicability of various isotherm models, Separ. Sci. Technol. 54 (6) (Apr. 2019) 943–961, https://doi.org/10.1080/01496395.2018.1526194.

[21] A. Naskar, A.K. Guha, M. Mukherjee, L. Ray, Adsorption of nickel onto *Bacillus cereus* M $^{1}_{16}$: a mechanistic approach, Separ. Sci. Technol. 51 (3) (Feb. 2016) 427–438, https://doi.org/10.1080/01496395.2015.1115069.

[22] Habib-ur-Rehman, M. Shakirullah, I. Ahmad, S. Shah, Hameedullah, Sorption studies of nickel ions onto sawdust of *dalbergia sissoo*, J. Chin. Chem. Soc. 53 (5) (Oct. 2006) 1045–1052, https://doi.org/10.1002/jccs.200600139.

[23] O. Ogunlalu, I.P. Oyekunle, K.O. Iwuozor, A.D. Aderibigbe, E.C. Emenike, Trends in the mitigation of heavy metal ions from aqueous solutions using unmodified and chemically-modified agricultural waste adsorbents, Curr. Res. Green Sustain. Chem. 4 (2021), 100188.

[24] M.A. Renu, K. Singh, S. Upadhyaya, R.K. Dohare, Removal of heavy metals from wastewater using modified agricultural adsorbents, Mater. Today Proc. 4 (9) (2017) 10534–10538.

[25] H.A. Hegazi, Removal of heavy metals from wastewater using agricultural and industrial wastes as adsorbents, HBRC J 9 (3) (2013) 276–282.

[26] H. Parab, M. Sudersanan, Engineering a lignocellulosic biosorbent–coir pith for removal of cesium from aqueous solutions: equilibrium and kinetic studies, Water Res. 44 (3) (2010) 854–860.

[27] A. Nawaz, B. Singh, P. Kumar, H3PO4-modified Lagerstroemia speciosa seed hull biochar for toxic Cr(VI) removal: isotherm, kinetics, and thermodynamic study, Biomass Convers. Biorefinery 13 (8) (Jun. 2023) 7027–7041, https://doi.org/10.1007/s13399-021-01780-8.

[28] K. Pyrzynska, Removal of cadmium from wastewaters with low-cost adsorbents, J. Environ. Chem. Eng. 7 (1) (2019), 102795.

[29] D.W. O'Connell, C. Birkinshaw, T.F. O'Dwyer, A modified cellulose adsorbent for the removal of nickel(II) from aqueous solutions, J. Chem. Technol. Biotechnol. 81 (11) (Nov. 2006) 1820–1828, https://doi.org/10.1002/jctb.1609.

[30] R. Ks, AF, biosorption of Co (II) metal by original and KMnO4 pretreated trapa natan biopolymer, Chem. Sci. J. 7 (4) (2016).

[31] M.N. Zafar, M. Saeed, R. Nadeem, S.H. Sumrra, S.S. Shafqat, M.A. Qayyum, Chemical pretreatments of Trapa bispinosa's peel (TBP) biosorbent to enhance adsorption capacity for Pb(ll), Open Chem. 17 (1) (2019) 325–336, https://doi.org/10.1515/chem-2019-0031.

[32] A.G. El-Said, Biosorption of Pb (II) ions from aqueous solutions onto rice husk and its ash, J. Am. Sci. 6 (10) (2010) 143–150.

[33] S. Gupta, S.K. Sharma, A. Kumar, Biosorption of Ni (II) ions from aqueous solution using modified Aloe barbadensis Miller leaf powder, Water Sci. Eng. 12 (1) (2019) 27–36.

[34] S. Gupta, A. Kumar, Removal of nickel (II) from aqueous solution by biosorption on A. barbadensis Miller waste leaves powder, Appl. Water Sci. 9 (4) (2019) 96, https://doi.org/10.1007/s13201-019-0973-1.

[35] C.T. Tovar, D. Acevedo, A.V. Ortíz, N.P. Gómez, M. Otero, Comparative study using raw and treated cassava and lemon residues in the removal of nickel (ii), Agrociencia 55 (2) (2021) 145–158.

[36] S. Asthana, A.O. Kedia, S. Gupta, Adsorption study of nickel Ni (II) ions from aqueous solution on tea waste [Online]. Available:, in: 3rd International Conference on Emerging Trends in Engineering and Management Research, 2017, pp. 67–77 https://www.researchgate.net/profile/Anil-Kedia/publication/330168090_Adsorption_Study_of_Nickel_Ni_II_Ions_from_Aqueous_Solution_on_Tea_Waste/links/5c30a8e6a6fdccd6b593e5aa/Adsorption-Study-of-Nickel-Ni-II-Ions-from-Aqueous-Solution-on-Tea-Waste.pdf. (Accessed 27 September 2023).

[37] G.O. El-Sayed, H.A. Dessouki, S.S. Ibrahim, Biosorption of Ni (II) and Cd (II) ions from aqueous solutions onto rice straw, Chem. Sci. J. 9 (2010) 1–11.

[38] M.A. Abdullah, A.D. Prasad, Biosorption of nickel (II) from aqueous solutions and electroplating wastewater using tamarind (Tamarindus indica L.) bark, Aust. J. Basic Appl. Sci. 4 (8) (2010) 3591–3601.

[39] M.A. Khan, M. Ngabura, T.S. Choong, H. Masood, L.A. Chuah, Biosorption and desorption of nickel on oil cake: batch and column studies, Bioresour. Technol. 103 (1) (2012) 35–42.

[40] Y. Gutha, V.S. Munagapati, S.R. Alla, K. Abburi, Biosorptive removal of Ni(II) from aqueous solution by *Caesalpinia bonducella* seed powder, Separ. Sci. Technol. 46 (14) (Sep. 2011) 2291–2297, https://doi.org/10.1080/01496395.2011.590390.

[41] V. Bharthi, et al., Pharmacognostical evaluation and phytochemical studies on Ayurvedic nutritional fruits of Trapa natans L, Int J Herb Med 3 (5) (2015) 13–19.

[42] C. Majee, R. Mazumder, G.S. Chakraborthy, A review on potential of plants under Trapa species, Int. J. Res. Pharm. Chem. 3 (2) (2013) 502–508.

[43] M. K. Hossain and S. M. Rahmatullah, "Potentiality of water chestnut (Trapa natans) in aquaculture of Bangladesh," Soc. Sci., vol. 7, no. 2, pp. 77–87..

[44] G.D. Singh, S. Singh, N. Jindal, A.S. Bawa, D.C. Saxena, Physico-chemical characteristics and sensory quality of Singhara (Trapa natans L.): an Indian water chestnut under commercial and industrial storage conditions, Afr. J. Food Sci. 4 (11) (2010) 693–702.

[45] W.-T. Tsai, et al., Conversion of water caltrop husk into torrefied biomass by torrefaction, Energy 195 (2020), 116967.

[46] M. Saeed, R. Nadeem, M. Yousaf, Removal of industrial pollutant (Reactive Orange 122 dye) using environment-friendly sorbent Trapa bispinosa's peel and fruit, Int. J. Environ. Sci. Technol. 12 (4) (2015) 1223–1234, https://doi.org/10.1007/s13762-013-0492-9.

[47] M.A. Qaiyum, J. Mohanta, R. Kumari, P.P. Samal, B. Dey, S. Dey, Alkali treated water chestnut *(Trapa natans L.)* shells *as a* promising phytosorbent for malachite green removal from water, Int. J. Phytoremediation 24 (8) (2022) 822–830, https://doi.org/10.1080/15226514.2021.1977912.

[48] M. Yousaf, R. Nadeem, M. Saeed, T. Zahoor, Fourier Transform infrared (FTIR) analysis of trapa bispinosa: a novel adsorbent for the removal of Cu (II) from aqueous solution in chemically treated form, J. Chem. Soc. Pak. 35 (6) (2013) 1474–1482.

[49] S. Kumar, S. Narayanasamy, R.P. Venkatesh, Removal of Cr(VI) from synthetic solutions using water caltrop shell as a low-cost biosorbent, Separ. Sci. Technol. 54 (17) (Nov. 2019) 2783–2799, https://doi.org/10.1080/01496395.2018.1560333.

[50] T. Yokoyama, et al., Basic properties and measuring methods of nanoparticles [Online]. Available:, in: Nanoparticle Technology Handbook, Elsevier, 2008, pp. 3–48 https://www.sciencedirect.com/science/article/pii/B9780444531223500040. (Accessed 28 September 2023).

[51] M. Geay, V. Marchetti, A. Clément, B. Loubinoux, P. Gérardin, Decontamination of synthetic solutions containing heavy metals using chemically modified sawdusts bearing polyacrylic acid chains, J. Wood Sci. 46 (4) (2000) 331–333, https://doi.org/10.1007/BF00766226.

[52] E. Kiefer, L. Sigg, P. Schosseler, Chemical and spectroscopic characterization of algae surfaces, Environ. Sci. Technol. 31 (3) (Mar. 1997) 759–764, https://doi.org/10.1021/es960415d.

[53] M.Z. Bin Mukhlish, Y. Horie, T. Nomiyama, Flexible alumina-silica nanofibrous membrane and its high adaptability in reactive red-120 dye removal from water, Water. Air. Soil Pollut. 228 (9) (2017) 371, https://doi.org/10.1007/s11270-017-3546-7.

[54] A. Aluigi, F. Rombaldoni, C. Tonetti, L. Jannoke, Study of Methylene Blue adsorption on keratin nanofibrous membranes, J. Hazard Mater. 268 (2014) 156–165.

[55] I. Langmuir, The constitution and fundamental properties of solids and liquids. Part I. Solids, J. Am. Chem. Soc. 38 (11) (Nov. 1916) 2221–2295, https://doi.org/10.1021/ja02268a002.

[56] G. McKay, Design models for adsorption systems in wastewater treatment, J. Chem. Technol. Biotechnol. 31 (1) (Jan. 1981) 717–731, https://doi.org/10.1002/jctb.503310197.

[57] S.Y. Elovich, O.G. Larinov, Theory of adsorption from solutions of non electrolytes on solid (I) equation adsorption from solutions and the analysis of its simplest form,(II) verification of the equation of adsorption isotherm from solutions, Izv Akad Nauk SSSR Otd Khim Nauk 2 (2) (1962) 209–216.

[58] D. Malwal, P. Gopinath, Efficient adsorption and antibacterial properties of electrospun CuO-ZnO composite nanofibers for water remediation, J. Hazard Mater. 321 (2017) 611–621.

[59] K. Fytianos, E. Voudrias, E. Kokkalis, Sorption–desorption behaviour of 2, 4-dichlorophenol by marine sediments, Chemosphere 40 (1) (2000) 3–6.

[60] Y. Tang, X. Liao, X. Zhang, G. Peng, J. Gao, L. Chen, Enhanced adsorption of hexavalent chromium and the microbial effect on quartz sand modified with Al-layered double hydroxides, Sci. Total Environ. 762 (2021), 143094.
[61] Q. Hu, Z. Zhang, Application of Dubinin–Radushkevich isotherm model at the solid/solution interface: a theoretical analysis, J. Mol. Liq. 277 (2019) 646–648.
[62] S.C. Gad, Nickel chloride, in: Reference Module in Biomedical Sciences, Elsevier, 2023, https://doi.org/10.1016/B978-0-12-824315-2.00704-1.
[63] E. Malkoc, Ni (II) removal from aqueous solutions using cone biomass of Thuja orientalis, J. Hazard Mater. 137 (2) (2006) 899–908.
[64] S.K. Lagergren, About the theory of so-called adsorption of soluble substances, Sven Vetenskapsakad Handingarl 24 (1898) 1–39.
[65] Y.-S. Ho, G. McKay, Sorption of dye from aqueous solution by peat, Chem. Eng. J. 70 (2) (1998) 115–124.
[66] M. Nasir, R.I. Sugatri, Characteristic of nanoparticle-chitosan system: solution and thin film study [Online]. Available:, in: IOP Conference Series: Earth and Environmental Science, IOP Publishing, 2018, 012001 https://iopscience.iop.org/article/10.1088/1755-1315/160/1/012001/meta. (Accessed 28 September 2023).
[67] A. Kapoor, T. Viraraghavan, Heavy metal biosorption sites in Aspergillus Niger, Bioresour. Technol. 61 (3) (1997) 221–227.
[68] H. Cai, X. Yang, Q. Cai, B. Ren, H. Qiu, Z. Yao, Lycium barbarum L. polysaccharide (LBP) reduces glucose uptake via down-regulation of SGLT-1 in Caco2 cell, Molecules 22 (2) (2017) 341.
[69] Y.-S. Yun, D. Park, J.M. Park, B. Volesky, Biosorption of trivalent chromium on the Brown seaweed biomass, Environ. Sci. Technol. 35 (21) (Nov. 2001) 4353–4358, https://doi.org/10.1021/es010866k.
[70] J. Arun, et al., In vitro antioxidant activities of an exopolysaccharide from a salt pan bacterium Halolactibacillus miurensis, Carbohydr. Polym. 155 (2017) 400–406.
[71] R.N. Shamma, M. Basha, Soluplus®: a novel polymeric solubilizer for optimization of carvedilol solid dispersions: formulation design and effect of method of preparation, Powder Technol. 237 (2013) 406–414.
[72] E. Malkoc, Y. Nuhoglu, Removal of Ni (II) ions from aqueous solutions using waste of tea factory: adsorption on a fixed-bed column, J. Hazard Mater. 135 (1–3) (2006) 328–336.
[73] K. Satyavani, S. Gurudeeban, T. Ramanathan, Influence of leaf broth concentration of Excoecaria agallocha as a process variable in silver nanoparticles synthesis, J. Nanomedicine Res. 1 (2) (2014) 11.
[74] M. Al-Amin, S.C. Dey, T.U. Rashid, M. Ashaduzzaman, S.M. Shamsuddin, Solar assisted photocatalytic degradation of reactive azo dyes in presence of anatase titanium dioxide, Int J Latest Res Eng Technol 2 (3) (2016) 14–21.
[75] A. Ananthi, D. Geetha, P.S. Ramesh, Preparation and characterization of silica material from rice husk ash–an economically viable method, Chem. Mater. Res. 8 (6) (2016) 1–7.
[76] A.M. Hofmeister, J.E. Bowey, Quantitative infrared spectra of hydrosilicates and related minerals, Mon. Not. Roy. Astron. Soc. 367 (2) (2006) 577–591.
[77] V. Šontevska, G. Jovanovski, P. Makreski, A. Raškovska, B. Šoptrajanov, Minerals from Macedonia. XXI. Vibrational spectroscopy as identificational tool for some phyllosilicate minerals, 2008, Acta Chim. Slov. 55 (4) (2008) 757–766 [Online]. Available: https://repository.ukim.mk/bitstream/20.500.12188/13927/1/XIII_1596.pdf. (Accessed 28 September 2023).
[78] A. Groza, A. Surmeian, Characterization of the oxides present in a polydimethylsiloxane layer obtained by polymerisation of its liquid precursor in corona discharge, J. Nanomater. 2015 (2015), 3–3.
[79] D.S. Volkov, O.B. Rogova, M.A. Proskurnin, Temperature dependences of IR spectra of humic substances of brown coal, Agronomy 11 (9) (2021) 1822.
[80] A. Fuad, U. Kultsum, A. Taufiq, E. Latifah, Nanostructural characters of β-SiC nanoparticles prepared from Indonesian natural resource using sonochemical method [Online]. Available:, in: Journal of Physics: Conference Series, IOP Publishing, 2018, 012066 https://iopscience.iop.org/article/10.1088/1742-6596/1011/1/012066/meta. (Accessed 28 September 2023).
[81] A.A. Borazan, D. Gokdai, Pine cone and boron compounds effect as reinforcement on mechanical and flammability properties of polyester composites, Open Chem. 16 (1) (May 2018) 427–436, https://doi.org/10.1515/chem-2018-0054.
[82] P. Wang, Q. Ma, D. Hu, L. Wang, Adsorption of methylene blue by a low-cost biosorbent: citric acid modified peanut shell, Desalination Water Treat. 57 (22) (May 2016) 10261–10269, https://doi.org/10.1080/19443994.2015.1033651.
[83] H. Zeng, et al., Preparation of Progesterone co-crystals based on crystal engineering strategies, Molecules 24 (21) (2019) 3936.
[84] F.L. Bernard, et al., Development of inexpensive cellulose-based sorbents for carbon dioxide, Braz. J. Chem. Eng. 36 (2019) 511–521.
[85] S. Gunasekaran, R.K. Natarajan, S. Natarajan, R. Rathikha, Structural investigation on curcumin, Asian J. Chem. 20 (4) (2008) 2903.
[86] P. Rajiv, A. Deepa, P. Vanathi, D. Vidhya, Screening for phytochemicals and FTIR analysis of Myristica dactyloids fruit extracts, Int. J. Pharm. Pharmaceut. Sci. (2017) 315–318.
[87] X. Zhao, H. Zhu, J. Chen, Q. Ao, FTIR, XRD and SEM analysis of ginger powders with different size: structure characteristic of ginger powders, J. Food Process. Preserv. 39 (6) (Dec. 2015) 2017–2026, https://doi.org/10.1111/jfpp.12442.
[88] J. Zhuang, M. Li, Y. Pu, A.J. Ragauskas, C.G. Yoo, Observation of potential contaminants in processed biomass using fourier transform infrared spectroscopy, Appl. Sci. 10 (12) (2020) 4345.
[89] C.G. Morisse, A.R. McInroy, C. Anderson, C.J. Mitchell, S.F. Parker, D. Lennon, Structure/activity relationships applied to the hydrogenation of α, β-unsaturated carbonyls: the hydrogenation of 3-butyne-2-one over alumina-supported palladium catalysts, Catal. Today 283 (2017) 110–118.
[90] N. Alizadeh, S. Shariati, N. Besharati, Adsorption of crystal violet and methylene blue on Azolla and fig leaves modified with magnetite iron oxide nanoparticles, Int. J. Environ. Res. 11 (2) (Jun. 2017) 197–206, https://doi.org/10.1007/s41742-017-0019-1.
[91] K. Das, C. Kendall, M. Isabelle, C. Fowler, J. Christie-Brown, N. Stone, FTIR of touch imprint cytology: a novel tissue diagnostic technique, J. Photochem. Photobiol., B 92 (3) (2008) 160–164.
[92] L.V. Bel'skaya, E.A. Sarf, D.V. Solomatin, Age and gender characteristics of the infrared spectra of normal human saliva, Appl. Spectrosc. 74 (5) (2020) 536–543.
[93] S. Wang, et al., Preparation of cellulose fibres with antibacterial Ag-loading nano-SiO2, Bull. Mater. Sci. 34 (4) (2011) 629–634, https://doi.org/10.1007/s12034-011-0173-6.
[94] K. Naseer, S. Ali, J. Qazi, ATR-FTIR spectroscopy as the future of diagnostics: a systematic review of the approach using bio-fluids, Appl. Spectrosc. Rev. 56 (2) (Feb. 2021) 85–97, https://doi.org/10.1080/05704928.2020.1738453.
[95] A. K. Vikas, G. Rajesh, A. M. Yusuf, K. Vishwanath, H. Jakeer, and B. Shridhar, "SYNTHESIS, CHARACTERIZATION, AND INVESTIGATION OF ELECTRICAL, MAGNETIC, SENSOR, AND MECHANICAL PROPERTIES OF POLYANILINE/ZINC DIOXIDE NANOCOMPOSITES", Accessed: September. 28, 2023. [Online]. Available: https://rasayanjournal.co.in/admin/php/upload/4039_pdf.pdf..
[96] H. Lin, et al., In situ IR study of surface hydroxyl species of dehydrated TiO 2: towards understanding pivotal surface processes of TiO 2 photocatalytic oxidation of toluene, Phys. Chem. Chem. Phys. 14 (26) (2012) 9468–9474.
[97] M. Thommes, et al., Physisorption of gases, with special reference to the evaluation of surface area and pore size distribution (IUPAC Technical Report), Pure Appl. Chem. 87 (9–10) (Oct. 2015) 1051–1069, https://doi.org/10.1515/pac-2014-1117.
[98] K.S.W. Sing, Reporting physisorption data for gas/solid systems with special reference to the determination of surface area and porosity (Recommendations 1984), Pure Appl. Chem. 57 (4) (Jan. 1985) 603–619, https://doi.org/10.1351/pac198557040603.
[99] G. Leofanti, M. Padovan, G. Tozzola, B. Venturelli, Surface area and pore texture of catalysts, Catal. Today 41 (1–3) (1998) 207–219.
[100] Md M.R. Khan, M.Z.B. Mukhlish, M.S.I. Mazumder, K. Ferdous, D.M.R. Prasad, Z. Hassan, Uptake of Indosol Dark-blue GL dye from aqueous solution by water hyacinth roots powder: adsorption and desorption study, Int. J. Environ. Sci. Technol. 11 (4) (May 2014) 1027–1034, https://doi.org/10.1007/s13762-013-0363-4.
[101] S. Gharbi, J. Khiari, B. Jamoussi, Studies, synthesis and characterization of chelation ion-exchange properties of copolymer resin derived from 8-hydroxyquinoline-formaldehyde-pyrogallol, Am. Chem. Sci. J. 4 (6) (2014) 874–889.
[102] H. Nassef, Y. Eltaweel, I. Awwad, Adsorption of nickel using activated carbon from sugarcane, Eng. Sci. Technol. Int. J. ESTIJ 7 (4) (2017) 11–18.

[103] J. de O. Primo, et al., Synthesis of zinc oxide nanoparticles by ecofriendly routes: adsorbent for copper removal from wastewater, Front. Chem. 8 (2020), 571790.
[104] H.N. Tran, S.-J. You, H.-P. Chao, Effect of pyrolysis temperatures and times on the adsorption of cadmium onto orange peel derived biochar, Waste Manag. Res. J. Sustain. Circ. Econ. 34 (2) (Feb. 2016) 129–138, https://doi.org/10.1177/0734242X15615698.
[105] T.W. Weber, R.K. Chakravorti, Pore and solid diffusion models for fixed-bed adsorbers, AIChE J. 20 (2) (Mar. 1974) 228–238, https://doi.org/10.1002/aic.690200204.
[106] P. Saha, S. Chowdhury, S. Gupta, I. Kumar, Insight into adsorption equilibrium, kinetics and thermodynamics of Malachite Green onto clayey soil of Indian origin, Chem. Eng. J. 165 (3) (2010) 874–882.
[107] N. Onursal, Y. Altunkaynak, A. Baran, M.C. Dal, Adsorption of nickel(II) ions from aqueous solutions using Malatya clay: equilibrium, kinetic, and thermodynamic studies, Environ. Prog. Sustain. Energy 42 (5) (Sep. 2023), e14150, https://doi.org/10.1002/ep.14150.
[108] B. Tekïn, U. Açikel, Adsorption isotherms for removal of heavy metal ions (copper and nickel) from aqueous solutions in single and binary adsorption processes, Gazi Univ. J. Sci. 36 (2) (2023) 495–509.
[109] C. Kamatchi, S. Arivoli, R. Prabakaran, Thermodynamic, kinetic, batch adsorption and isotherm models for the adsorption of nickel from an artificial solution using chloroxylon swietenia activated carbon, Phys. Chem. Res. 10 (3) (2022) 315–324.
[110] R. Chanda, A.H. Mithun, M.A. Hasan, B.K. Biswas, Nickel removal from aqueous solution using chemically treated mahogany sawdust as biosorbent, J. Chem. 2021 (2021) 1–10.
[111] P. Rani, R. Johar, P.S. Jassal, Adsorption of nickel (II) ions from wastewater using glutaraldehyde cross-linked magnetic chitosan beads: isotherm, kinetics and thermodynamics, Water Sci. Technol. 82 (10) (2020) 2193–2202.
[112] D. Liu, Y. Zhu, Z. Li, D. Tian, L. Chen, P. Chen, Chitin nanofibrils for rapid and efficient removal of metal ions from water system, Carbohydr. Polym. 98 (1) (2013) 483–489.
[113] V.K. Gupta, A. Nayak, S. Agarwal, M. Chaudhary, I. Tyagi, Removal of Ni (II) ions from water using scrap tire, J. Mol. Liq. 190 (2014) 215–222.
[114] R. Katal, E. Hasani, M. Farnam, M.S. Baei, M.A. Ghayyem, Charcoal ash as an adsorbent for Ni(II) adsorption and its application for wastewater treatment, J. Chem. Eng. Data 57 (2) (2012) 374–383, https://doi.org/10.1021/je200953h.
[115] X. Guo, S. Zhang, X. Shan, Adsorption of metal ions on lignin, J. Hazard Mater. 151 (1) (2008) 134–142.
[116] A. Thevannan, R. Mungroo, C.H. Niu, Biosorption of nickel with barley straw, Bioresour. Technol. 101 (6) (2010) 1776–1780.
[117] Y. Hannachi, N.A. Shapovalov, A. Hannachi, Adsorption of Nickel from aqueous solution by the use of low-cost adsorbents, Kor. J. Chem. Eng. 27 (1) (Jan. 2010) 152–158, https://doi.org/10.1007/s11814-009-0303-7.
[118] B.H. Hameed, A.A. Ahmad, N. Aziz, Adsorption of reactive dye on palm-oil industry waste: equilibrium, kinetic and thermodynamic studies, Desalination 247 (1) (Oct. 2009) 551–560, https://doi.org/10.1016/j.desal.2008.08.005.
[119] S. Sahu, N. Bishoyi, R.K. Patel, Cerium phosphate polypyrrole flower like nanocomposite: a recyclable adsorbent for removal of Cr (VI) by adsorption combined with in-situ chemical reduction, J. Ind. Eng. Chem. 99 (2021) 55–67.
[120] H. Veselá, E. Šucman, Determination of acrylamide in food using adsorption stripping voltammetry, Czech J. Food Sci. 31 (4) (2013) 401–406.
[121] G. Li, J. Ye, Q. Fang, F. Liu, Amide-based covalent organic frameworks materials for efficient and recyclable removal of heavy metal lead (II), Chem. Eng. J. 370 (2019) 822–830.
[122] N.A. Sánchez-Flores, et al., Behavior of Ni(II) and Mn(II) in single and binary aqueous solutions in the adsorption process by rice hull ashes (RHA), Separ. Sci. Technol. 52 (15) (Oct. 2017) 2407–2414, https://doi.org/10.1080/01496395.2017.1355924.
[123] E. Soćo, J. Kalembkiewicz, Adsorption of nickel (II) and copper (II) ions from aqueous solution by coal fly ash, J. Environ. Chem. Eng. 1 (3) (2013) 581–588.
[124] P.P. Vishwakarma, K.P. Yadava, V.N. Singh, Nickel (II) removal from aqueous solutions by adsorption on fly ash, Pertanika 12 (3) (1989) 357–366.
[125] J.O. Ighalo, F.O. Omoarukhe, V.E. Ojukwu, K.O. Iwuozor, C.A. Igwegbe, Cost of adsorbent preparation and usage in wastewater treatment: a review, Clean. Chem. Eng. (2022), 100042.